NASA Contractor Report 181855

ICASE Report No. 89–32

ICASE

INVISCID SPATIAL STABILITY OF A COMPRESSIBLE MIXING LAYER. PART III. EFFECT OF THERMODYNAMICS

T. L. Jackson
C. E. Grosch

Contract No. NAS1–18605
June 1989

Institute for Computer Applications in Science and Engineering
NASA Langley Research Center
Hampton, Virginia 23665–5225

Operated by the Universities Space Research Association

National Aeronautics and Space Administration

Langley Research Center
Hampton, Virginia 23665-5225

INVISCID SPATIAL STABILITY OF A COMPRESSIBLE MIXING LAYER PART III. EFFECT OF THERMODYNAMICS

T. L. Jackson

Department of Mathematics and Statistics
Old Dominion University
Norfolk, Virginia 23529

C. E. Grosch

Department of Oceanography and
Department of Computer Science
Old Dominion University
Norfolk, Virginia 23529

Abstract. We report the results of a comprehensive comparative study of the inviscid spatial stability of a parallel compressible mixing layer using various models for the mean flow. The models are (a) the hyperbolic tangent profile for the mean speed and the Crocco relation for the mean temperature, with the Chapman viscosity-temperature relation and a Prandtl number of one; (b) the Lock profile for the mean speed and the Crocco relation for the mean temperature, with the Chapman viscosity-temperature relation and a Prandtl number of one; and (c) the similarity solution for the coupled velocity and temperature equations using the Sutherland viscosity temperature relation and arbitrary but constant Prandtl number. The purpose of this study was to determine the sensitivity of the stability characteristics of the compressible mixing layer to the assumed thermodynamic properties of the fluid. It is shown that the qualitative features of the stability characteristics are quite similar for all models but that there are quantitative differences resulting from the difference in the thermodynamic models. In particular, we show that the stability characteristics are sensitive to the value of the Prandtl number.

This work was supported by the National Aeronautics and Space Administration under NASA Contract NAS1-18605 while the authors were in residence at the Institute for Computer Applications in Science and Engineering, NASA Langley Research Center, Hampton, VA 23665.

1. Introduction. The study of the stability of compressible shear flows is somewhat more complicated than that of incompressible shear flows in that the thermodynamics of the compressible fluid is of major importance. As a consequence of compressibility the types of disturbances which can exist are quite varied: they can be subsonic, sonic, or supersonic modes and these can be either vorticity or acoustic modes (Mack, 1989); there can be multiple unstable modes with the same frequency; and finally three dimensional modes are of great importance because they may be more unstable than two dimensional modes; the characteristics of these modes are dependent upon the thermodynamics choosen.

The basic formulation of the theory of the stability of compressible shear flows, both wall bounded and free, is due to Lees and Lin (1946), and Dunn and Lin (1955) first showed the importance of three dimensional disturbances. The major additional effort in this area appears to be directed towards understanding the stability characteristics of compressible boundary layers (see Mack; 1965, 1984, and 1987 for comprehensive reviews) with much less effort devoted to understanding the stability characteristics of compressible free shear layers.

The earliest calculations of stability characteristics of compressible boundary layers used realistic thermodynamic relations (Brown, 1962, Lees and Reshotko, 1962, and Mack, 1965) and this has continued to be the practice to the present day. The situation with regard to stability calculations for free shear layers is quite different. Most studies of the stability of compressible free shear flows have been based on assumed, somewhat arbitrary, mean velocity and temperature profiles which are not solutions to the mean flow equations but do satisfy the boundary conditions. If both the velocity and temperature profiles are arbitrary it might be conjectured that the solutions of the stability problem could be unrelated to those of the physical problem. If they are, at least, rough approximations to the actual solutions, one might conjecture that the solutions of the model stability problem would approximate those of physical problem. These solutions of the model problems might be useful in elucidating qualitative features of the true stability problem because they are easier to treat. Some examples of studies of this type are that of Gill (1965), who studied the temporal stability of "top hat" jets and wakes and those of Blumen (1970); Blumen, Drazin and Billings (1975), and Drazin and Davey (1977) who examined the temporal stability of a compressible mixing layer with the mean velocity profile assumed to be given by a hyperbolic tangent and a constant temperature.

In most compressible free shear stability studies the thermodynamics used was that of the model fluid (Stewartson, 1964). This model was originally introduced in order to simplify the thermodynamics of the flow in compressible boundary layers. In addition to obeying the perfect gas law (valid for real gases at temperatures less than a few thousand degrees K), the model fluid has a unit Prandtl number so that the rates of diffusion of heat and momentum are equal, and the Chapman (1950) viscosity law with the viscosity proportional to the temperature is assumed to be valid. One class of approximate solutions involves modeling the mean velocity profile by a hyperbolic tangent and using the Crocco relation for the mean temperature profile. This approximation has been used by a number of authors, including Ragab and Wu (1988), Tam and Hu (1988), and Zhuang, Kubota and Dimotakis (1988). We have also used this model in a comprehensive study of the spatial stability of a compressible mixing layer (Jackson and Grosch, 1988; hereafter referred to as Part I) as well as in a similar study of a reacting compressible mixing layer (Jackson and Grosch, 1989).

Another class of models can be defined as those which use the Lock profile (Lock, 1951), the similarity solution for the velocity profile with the viscosity proportional to the temperature, a Prandtl number of

unity and various temperature profiles. Lessen, Fox and Zien (1965, 1966) in temporal stability calculations used the Lock profile and assumed that the flow was iso-energetic so that the temperature of the stationary gas was much greater than that of the moving gas even at moderately supersonic speeds. Gropengiesser (1969) used a generalized hyperbolic tangent profile (see his equation (2.27)) to approximate the Lock profile and used the Crocco relation for the temperature in spatial stability calculations.

The final class of solutions to the mean flow equations are those where the Prandtl number is not necessarily one and a reasonably realistic viscosity-temperature relation, such as the Sutherland law, is used. The velocity and temperature profiles are exact similarity solutions of the mean flow equations. Quite surprisingly, there are few linear stability calculations for compressible mixing layers with these more realistic mean velocity and temperature profiles. The only published results, of which we know, are those of Ragab and Wu (1988) for spatial stability and those of Macaraeg, Street and Hussaini (1988) for temporal stability. It seems that the main interest of Ragab and Wu was to determine the dependence of the maximum growth rate of the disturbances on the velocity ratio of the mixing layer for subsonic flows. They concluded that the maximum growth rate depends on the velocity ratio in a complex way, with the maximum growth rate appearing at a particular nonzero velocity ratio. Macaraeg, et al studied the temporal stability of a compressible mixing layer for a few selected values of the Mach number (≤ 4), and a few values of the free stream temperature ratio. They were the first to point out the sensitivity of the stability characteristics of this class of flows to variations in the Prandtl number.

Very recently there has been a revival of interest in the stability of compressible free shear layers, particularly at supersonic speeds. An unanswered question is the accuracy of the results of those calculations in which various models of the mean flow thermodynamics have been used. It is clear that there will be quantitative differences in, for example, phase speeds and growth rates of the disturbances depending on the model of the mean flow. The important questions are first, the extent to which *qualitative predictions* of recent, and older, studies are dependent on the models of the mean velocity and temperature used, and second, the *magnitude of the differences* in the quantitative predictions as a function of the mean flow model.

In order to answer these questions we undertook a comprehensive systematic study of the stability of one free shear flow, the compressible mixing layer. In this study we calculated the stability characteristics of the compressible mixing layer using a number of representative models of the mean velocity and temperature profiles over a wide range of Mach numbers. The models are (a) the hyperbolic tangent profile for the mean speed and the Crocco relation for the mean temperature, with the Chapman viscosity-temperature relation and a Prandtl number of one; (b) the Lock profile for the mean speed and the Crocco relation for the mean temperature, with the Chapman viscosity-temperature relation and a Prandtl number of one; and (c) the similarity solution for the coupled velocity and temperature equations using the Sutherland viscosity temperature relation and arbitrary but constant Prandtl number. In section 2 we formulate the problem, including defining the thermodynamic models. Our results are presented in section 3. Finally, we summarize our conclusions in section 4.

2. Formulation of the Problem.

2.1. The Mean Flow The problem considered here is the inviscid spatial stability of the steady two dimensional flow of a compressible mixing layer which lies between two streams with different speeds and

temperatures. We take one of the streams to be moving at $+\infty$ and the other to be stationary at $-\infty$. The equations are nondimensionalized by the values of the density, temperature, and speed in the moving stream. The length scale is a characteristic length of the mean flow, and the time scale is the ratio of the length and speed scales. The x axis is along the direction of flow, the y axis is normal to the flow direction, and the z axis is in the cross stream direction. U and V are the velocity components in the x and y directions, respectively, ρ is the density, and T the temperature. We assume that the equations governing the mean flow are the compressible boundary layer equations (Stewartson, 1964).

These equations are transformed into the incompressible form by the Howarth-Dorodnitzyn transformation

$$Y = \int_0^y \rho \, dy, \qquad \hat{V} = \rho V + U \int_0^y \rho_x \, dy. \tag{2.1a,b}$$

Because the pressure gradient is zero,

$$\rho T = 1. \tag{2.2}$$

Assuming that the mean flow is given by a similarity solution, we transform to the similarity variable

$$\eta = \frac{Y}{2\sqrt{x}}. \tag{2.3}$$

With

$$U = f'(\eta), \tag{2.4}$$

the equations for the mean flow quantities U and T reduce to

$$\left[\frac{\mu}{T} f''\right]' + 2ff'' = 0, \tag{2.5}$$

$$\left[\frac{\mu}{Pr\ T} T'\right]' + 2fT' + (\gamma - 1) M^2 \left[\frac{\mu}{T}\right] (f'')^2 = 0, \tag{2.6}$$

where the primes indicates differentiation with respect to η. Here μ is the viscosity coefficient, Pr is the Prandtl number, γ is the ratio of specific heats of the gas, and M the Mach number of the moving stream.

The mean flow field is found by solving equations (2.5) and (2.6) subject to the boundary conditions,

$$f'(+\infty) = 1, \qquad T(+\infty) = 1, \tag{2.7a,b}$$

and

$$f'(-\infty) = 0, \qquad T(-\infty) = \beta_T, \tag{2.8a,b}$$

with β_T the ratio of the temperature in the stationary gas to that of the moving gas. If β_T is less than one, the stationary stream is relatively cold compared to the moving stream, and if β_T is greater than one it is

relatively hot.

It should be noted that equations (2.5) through (2.8) constitute a fifth order boundary value problem, but that there are only four boundary conditions. Ting (1959) has shown that an appropriate boundary condition can be obtained by matching the freestream pressures on either side of the mixing layer if at least one of the streams is supersonic. However, Klemp and Acrivos (1972) have shown that this condition is incomplete if both streams are subsonic. These conditions are equivalent to a specification of $f(-\infty)$. This value, a specification of the stream function, can be varied so as to ensure that $f(0)$ takes on any particular value. This will not effect the physics of the flow, only the location of the origin of the coordinate system.

The structure of the mean flow clearly depends on the variation of μ and Pr with temperature and pressure. In general, both μ and Pr are very weakly dependent on pressure and can be taken to be independent of pressure. The Prandtl number is somewhat dependent on the temperature but, for this study, will be assumed to be constant, with calculations being carried out over a range of Pr between 0.7 and 1.0. Finally, the dependence of viscosity on temperature is quite important and the choice of that dependence leads to several thermodynamic models discussed in the following section.

2.2. Flow Models Given a value of Pr and $\mu(T)$ the mean flow is determined by the solution to equations (2.5) and (2.6) with the boundary conditions (2.7) and (2.8) and a specification of $\dot{f}(0)$. We will consider three models for the mean flow.

If it is assumed that the viscosity is proportional to the temperature, that is we use the Chapman viscosity law, equation (2.5) is uncoupled from (2.6). With Pr = 1, equation (2.6) can be solved in closed form to give the Crocco relation, which with the boundary conditions (2.7) and (2.8), is given by

$$T = 1 - (1-\beta_T)(1-U) + \frac{\gamma-1}{2} M^2 U (1-U). \tag{2.9}$$

The first model of the mean flow involves using (2.9) for the mean temperature profile and approximating the mean velocity profile by a hyperbolic tangent

$$U = \frac{1}{2}(1 + tanh(\eta)). \tag{2.10}$$

We will call this approximation the Tanh model. The results for this model were presented in Part I. Some of these results will be reproduced here for ease of reference and comparison purposes.

The second model of the mean flow again uses (2.9) for the mean temperature profile, and the solution to (2.5) with μ proportional to T and Pr = 1, for the mean velocity profile. We will call this the Lock model.

The third model is one in which the Prandtl number is constant but not necessarily one and a reasonably realistic viscosity-temperature relation is used. For temperatures greater than about 100 K^o, a Sutherland type of relation

$$\mu = a\, T^{3/2} / (b + T), \quad a = 1 + b, \quad b = 110.4 K^o / T^*, \tag{2.11}$$

with T^* the reference temperature, is reasonably accurate. The mean velocity and temperature profiles are the solutions of (2.5) to (2.8) and μ given by (2.11). We will call this the Sutherland model.

2.3. The Stability Problem The stability problem can be formulated independently of the detailed form of the U and T profiles. The flow field is perturbed by introducing two dimensional wave disturbances in the velocity, pressure, temperature and density with amplitudes which are functions of η. For example, the pressure perturbation is

$$p = \Pi(\eta)\, exp\,[i\,(\alpha x - \omega t)], \tag{2.12}$$

with Π the amplitude, α the complex wavenumber and ω the frequency which is taken to be real because we are only treating the spatial stability problem. Substituting the expression (2.12) for the pressure perturbation and similar expressions for the other flow quantities into the inviscid compressible equations yields the ordinary differential equations for the perturbation amplitudes. It is straightforward to derive a single equation governing Π, given by

$$\Pi'' - \frac{2U'}{U-c}\Pi' - \alpha^2 T\,[T - M^2(U-c)^2]\,\Pi = 0, \tag{2.13}$$

where c is the complex phase speed

$$c = \frac{\omega}{\alpha}, \tag{2.14}$$

and primes indicate differentiation with respect to the similarity variable η. Since α is complex, the real part of α is the wave number in the x direction, while the imaginary part of α indicates whether the disturbance is amplified, neutral, or damped depending on whether α_i is negative, zero, or positive. The phase speed, c_{ph}, is given by ω / α_r. If α_i is zero, $c = c_N$ is the phase speed of a neutral mode.

The boundary conditions for Π are obtained by considering the limiting form of equation (2.13) as $\eta \to \pm\infty$. The solutions to (2.13) are of the form

$$\Pi \to exp\,(\pm\Omega_\pm \eta), \tag{2.15}$$

where

$$\Omega^2_+ = \alpha^2[1 - M^2(1-c)^2], \qquad \Omega^2_- = \alpha^2\beta_T\,[\beta_T - M^2 c^2]. \tag{2.16}$$

We define $c_\pm$ to be the values of the phase speed for which $\Omega^2_\pm$ vanishes. Thus,

$$c_+ = 1 - \frac{1}{M}, \qquad c_- = \frac{\sqrt{\beta_T}}{M}. \tag{2.17}$$

Note that c_+ is the phase speed of a sonic disturbance in the moving stream and c_- is the phase speed of a sonic disturbance in the stationary stream. At

$$M = M_* \equiv 1 + \sqrt{\beta_T} \tag{2.18}$$

$c_\pm$ are equal, and this value is denoted $\hat{c}$.

The nature of the disturbances and the appropriate boundary conditions can now be illustrated by reference to Figure 1, where we plot $c_\pm$ versus M. In what follows we assume that $\alpha^2_r > \alpha^2_i$. These curves divide the $c_r - M$ plane into four regions, where c_r is the real part of c. If a disturbance exists with a M and c_r in region 1, then Ω^2_+ and Ω^2_- are both positive, and the disturbance is subsonic at both boundaries. In region 3, both Ω^2_+ and Ω^2_- are negative and hence the disturbance is supersonic at both boundaries. In region 2, Ω^2_+ is positive and Ω^2_- is negative, and the disturbance is subsonic at $+\infty$ and supersonic at $-\infty$, and we classify it as a fast mode. Finally, in region 4, Ω^2_+ is negative and Ω^2_- is positive so the disturbance is supersonic at $+\infty$ and subsonic at $-\infty$, and we classify it as a slow mode.

One can now see that the appropriate boundary condition for either damped or outgoing waves in the moving and stationary streams are, respectively,

$$\Pi \to e^{-\Omega_+ \eta}, \quad \text{if } c_r > c_+, \qquad \Pi \to e^{-i\eta\sqrt{-\Omega^2_+}}, \quad \text{if } c_r < c_+, \tag{2.19a}$$

$$\Pi \to e^{\Omega_- \eta}, \quad \text{if } c_r < c_-, \qquad \Pi \to e^{-i\eta\sqrt{-\Omega^2_-}}, \quad \text{if } c_r > c_-. \tag{2.19b}$$

To solve the disturbance equation (2.13), we first transform it to a Riccati equation by setting

$$G = \frac{\Pi'}{\alpha T \Pi}. \tag{2.20}$$

Thus, (2.13) becomes

$$G' + \alpha T G^2 - [\frac{2U'}{U-c} - \frac{T'}{T}] G = \alpha [T - M^2 (U-c)^2]. \tag{2.21}$$

The boundary conditions can be found from (2.19) and (2.20).

The stability problem is thus to solve equation (2.21) for a given real frequency ω and Mach number M. The eigenvalue is the wavenumber α. Because this equation has a singularity at $U = c_N$, we integrate it along the complex contour $(\eta_-,-1)$ to $(0,-1)$ and $(\eta_+,-1)$ to $(0,-1)$ using a variable step Runge-Kutta scheme. In our calculations we have taken $\eta_\pm$ to be 6 for the Tanh and Lock profiles. However, we found that η_- needs to be larger for the Sutherland model because the decay at $-\infty$ is slower than for the other two models, with the rate of decay decreasing as β_T is decreased (Mack, 1989). We choose an initial value of α and compute the boundary conditions from (2.19). We then iterate on α, using Muller's method, until the boundary conditions are satisfied and the jump in G at $(0,-1)$ is less than 10^{-6}. All calculations were done in 64 bit precision.

3. Results. In this section we present results for the regularity condition, phase speeds, growth rates, and eigenfunctions of the stability problem. In all of our calculations we have taken $\gamma = 1.4$ and $0 \le M \le 7$. The choice of a maximum value of 7 for M is based on the results of our previous calculations for the Tanh profile wherein we took $0 \le M \le 10$, (Part I). It is clear from these results that the asymptotic ($M \to \infty$) behavior of the solutions to the stability problem are apparent by Mach 7. Finally, we have taken the reference temperature T^* to be $1500 K^o$. We have also carried out stability calculations for values of T^* of $500 K^o$ and $1000 K^o$ and found at most only a 2% change in the eigenvalues. Thus, we conclude that the actual value of the reference temperature T^* is not the important parameter, rather it is the

ratio of the temperatures in the stationary stream to that of the moving stream β_T which is the important parameter.

3.1 The Regularity Condition. The Lees and Lin (1946) regularity condition is given by

$$S(\eta) \equiv \frac{d}{d\eta}\left(T^{-2}\frac{dU}{d\eta}\right). \tag{3.1}$$

Let η_c be a root of $S(\eta)$, and define $\bar{c} = U(\eta_c)$. If $\bar{c}$ lies in region 1 of the $c_r - M$ diagram, then Lees and Lin (1946) have shown that $\bar{c} = c_N$ is the phase speed of a true neutral mode. The corresponding neutral wave number and frequency must be determined numerically. These modes are called subsonic neutral modes. It has been used by number of authors, for example, Lessen, et al. (1965), Gropengiesser (1969), Jackson and Grosch (1988), and Macaraeg, et al. (1988), to find the phase speed of subsonic neutral modes. If $\bar{c}$ lies in regions 2, 3, or 4 of the $c_r - M$ diagram, then $\bar{c}$ does *not* correspond to the phase speed of a true neutral mode. The phase speeds in these regions must be found numerically.

Figures (2-5) are plots of $S(\eta)$ versus η for the three thermodynamic models, particular values of β_T and Pr, and Mach numbers of 3 and 5. All of these curves have been normalized so that their maximum is one. All of these plots show similar behavior; S has a single root at Mach 3, but three roots at Mach 5. This is quite apparent for the Tanh, Lock, and Sutherland profiles with Pr = 1 but is not so readily apparent for the Sutherland profile with Pr = 0.7 because of the scale. However, there are a pair of zeros of S in the interval [-2,0].

We have shown in Part I, for the Tanh profile, that S is a cubic in $\tanh(\eta)$ and therefore has either one or three real roots. There is one real root for $M < M_o$ and three real roots for $M \geq M_o$, where M_o is given by (3.6) of Part I. This is illustrated in Figure 6 for $\beta_T = 1$, with the dashed curves the sonic curves. We see that one root, that which exists at Mach zero, has a constant value of $\bar{c} = 0.5$. The other two roots form a "bubble" for Mach numbers greater than M_o. The bubble is symmetric because of the symmetry of the mean profiles. We note here from Part I that if $\beta_T > 1$, the value of $\bar{c}$ for the single root is a monotonic curve greater than 1/2, with a bubble below it. Also, if $\beta_T < 1$, the value of $\bar{c}$ for the single root is also a monotonic curve less than 1/2, with the bubble now appearing above it. Thus at $\beta_T = 1$ there is a saddle point in the $\bar{c} - M$ plane. This value of β_T, which we denote by $\hat{\beta}_T$, plays a critical role in the behavior of the solutions of the stability problem, as will be shown below. The corresponding value of the root which appears at Mach zero is denoted by $\hat{c}$.

We have not been able to demonstrate these properties analytically for the Lock and Sutherland profiles, but have been able to do so numerically. Some of the numerical evidence is presented in Figures 7-9 where we plot $\bar{c}$ versus M for the different thermodynamic models and values of β_T. The dashed curves are the sonic curves, shown for reference. Results are shown for the Lock profile in Figure 7 for the saddle point value of $\hat{\beta}_T = 0.57753$. The surface is not symmetric about the line $\hat{c} = 0.4318$ because the Lock profile is slightly asymmetric about $\eta = 0$. Figures 8 and 9 show results for the Sutherland model with Pr = 1 (Figure 8) and 0.7 (Figure 9). In both figures the monotonic curve and the bubble are visible with asymmetries caused by the asymmetry of the Sutherland profile. In both cases the value of β_T was chosen to be close to the saddle point value $\hat{\beta}_T$. Since the mean profiles are now coupled through the viscosity, the exact saddle point value is difficult to determine numerically. From Figures 8 and 9 it is clear that the value of $\hat{\beta}_T$ is strongly dependent on the value of the Prandtl number. The dependence on Pr is shown very

clearly in the results presented in Figures 10 and 11. Figure 10 is a plot of $\hat{\beta}_T$ for the Sutherland profile as a function of the Prandtl number. As the Prandtl number is decreased from one, the saddle point value decreases dramatically. Figure 11 shows the variation of the corresponding $\hat{c}$ with Prandtl number. This value also decreases as the Prandtl number decreases.

For all three thermodynamic models the three real roots of S always lie in regions 2, 3, or 4 for two dimensional modes. Therefore, for a two dimensional mode, only the single root which lies in region 1 is the phase speed of a true neutral mode. However, the sonic speeds $c_\pm$ are functions of the angle of propogation of the waves (M is replaced by M cos θ in (2.17)), and as the angle is increased, the sonic curves shift towards higher Mach numbers thus increasing the extent of region 1. It is therefore clear that there will be some angle of propagation for which all three zeros of S lie in region 1. For this angle and all greater angles less than 90^0, all three zeros of S yield the phase speed of true neutral subsonic modes.

3.2 Neutral modes. In this section we present the phase speeds, frequencies, and wavenumbers of the neutral modes for the three models with β_T of 2.0, 1.0, and 0.5 and Pr = 0.7 for the Sutherland model.

Figure 12 shows plots of the phase speeds of the neutral modes as a function of Mach number for $\beta_T = 2$ obtained by using the Tanh, Lock, and Sutherland models. The results for all three models show qualitatively similar behavior and small quantitative differences. It should be noted that β_T of 2.0 is considerably larger than the saddle point value of $\hat{\beta}_T$ for all three models. As the Mach number is increased past M_s, the Mach number at which the phase speed equals that of the sonic wave, the subsonic neutral mode in region 1 is transformed into a fast supersonic neutral mode in region 2. At M_* a slow supersonic neutral mode appears in region 4. There are some quantitative differences between the results using the different models. For example, in region 1, the neutral mode of the Tanh model has the lowest phase speed and that of the Lock model the highest with the phase speed of the Sutherland model in between. However there is only about a 10% maximum difference in the phase speeds. The same ordering with respect to magnitude of the phase speed is also true for the fast supersonic neutral mode in region 2. The phase speeds of the slow supersonic neutral modes in region 4 are very nearly the same for all of the models over the range of Mach numbers shown. The corresponding wave numbers of the neutral modes are plotted in Figure 13 and the corresponding frequencies in Figure 14. The magnitudes of α_N and ω_N are similar for all of the models for the slow modes appearing in region 4. The neutral wave numbers and frequencies of the fast modes for all models eventually increases with increasing Mach number, while those of the slow modes decrease in this range of Mach numbers.

Similar results are shown in Figures 15-17 for $\beta_T = 1.0$. The phase speed of the neutral modes are plotted in Figure 15 and one can see a marked difference between the results for the Tanh model and the others. This is due to the fact that β_T of one is the saddle point value for the Tanh model while $\hat{\beta}_T$ occurs at a considerably lower value for the other models. Thus the phase speeds of the neutral modes increases for the Lock and Sutherland models as M increases, while that of the Tanh model is constant. At M_s, the phase speeds of the Lock and Sutherland models are transformed from subsonic to fast supersonic neutral models. In contrast, the subsonic neutral mode of the Tanh profile is split at $M_s = M_*$ into both fast and slow supersonic neutral modes. Figure 16 is a plot of the corresponding wavenumbers of the neutral modes. For $M > M_*$, the Tanh model yields values of α_N which are equal for both the fast and slow supersonic neutral modes. This is due to the fact that the mean profiles of both velocity and temperature are symmetric about $\eta = 0$. Beyond this, all of the models yield neutral wavenumbers which have the same general

behavior with increasing Mach number. Finally, the variation of the frequency of the neutral modes, ω_N, as a function of Mach number is shown in Figure 17. If $M<M_*$ then ω_N is essentially independent of the thermodynamic model. For $M>M_*$, all three models yield similar behavior.

Finally, Figures 18-20 show the variation of the phase speed, wavenumber, and frequency of the neutral wave with Mach number for $\beta_T = 0.5$. This value of β_T is less than the saddle point value for the Tanh (= 1.0) and the Lock (≈ 0.57753) models but substantially greater than the saddle point value of the Sutherland model (≈ 0.145). Because of this, the results from the Tanh and Lock models are similar and both differ from those of the Sutherland model. In region 1 of Figure 18 the neutral phase speed obtained from the Tanh and Lock models is less than $\hat{c}$ because a β_T of 0.5 is less than the saddle point value for these models. The opposite is true for the Sutherland model. Further, in this region the c_N value for the Tanh model is smaller than that of the Lock model because a β_T of 0.5 is considerably smaller than the saddle point value for the Tanh model and only slightly smaller than that of the Lock model. Because the β_T of 0.5 is smaller than the saddle point values for the Tanh and Lock models the subsonic neutral modes of these models are transformed into slow supersonic neutral modes at M_s and fast supersonic neutral modes appear at M_*. Conversely, the subsonic neutral mode for the Sutherland model is transformed to a fast supersonic neutral mode at M_s, while a slow supersonic neutral mode appears at M_*. In regions 2 and 4 it can be seen that the phase speeds of the fast and slow supersonic neutral modes are quite similar for all models.

The variation of the neutral wave number with Mach number is shown in Figure 19. It is apparent from the results shown in this figure, and those of Figures 13 and 16, that α_N increases in the subsonic region with decreasing values of β_T. The Tanh model has the largest rate of change, followed by the Lock model with the Sutherland model having the smallest rate of change. In contrast to the results for the other values of β_T, the slow supersonic neutral mode of the Tanh model has a larger wavenumber than that of the fast supersonic neutral mode. The wavenumbers of the neutral supersonic modes are roughly equal for the Lock model. At larger values of the Mach number, α_N increases with increasing Mach number for all cases except that of the slow supersonic mode of the Sutherland model. Also, Figure 20 shows the change in the frequency of the neutral modes with Mach number. The behavior is qualitatively similar to that found for other values of β_T.

Figures 21 thru 23 are plots of selected two dimensional slow supersonic neutral eigenfunctions for $\beta_T = 1$ and Mach 5. These plots show the variation of Π with η_r on the contour $\eta_i = -1$. All of these have been normalized so that the maximum of the absolute value of Π is unity. All show a rapid phase shift near the center of the mixing layer. Because these are slow supersonic neutral modes they have exponential decay at $\eta = -\infty$ and oscillate with constant amplitude and linear phase at $\eta = \infty$. The exponential decay is the slowest in the Sutherland model and most rapid in the Tanh model. The Sutherland model also yields the slowest rate of change in the supersonic region. Despite these quantitative differences, the eigenfunctions obtained from all the models are qualitatively similar.

3.3 Growth rates. The growth rates of the unstable modes are presented in this section and compared as a function of Mach number and β_T for the three models. In addition the variation of the growth rate with frequency for $\beta_T = 2.0$ is presented at selected values of the Mach number. It should be noted that the phase speeds of the unstable modes lie in the vicinity of the phase speed of the neutral mode in region 1 and between the phase speeds of the neutral modes and the corresponding sonic curves in regions 2

and 4. Thus we see that at any given Mach number there is only a small band of phase speeds of the unstable modes.

Figure 24 shows the maximum growth rates versus Mach number for $\beta_T = 2.0$. The general variation is similar for all of the models. The maximum growth rate is largest at Mach zero and decreases by a factor of 5 to 10 as the Mach number increases from zero to M_* and approaches a limiting value as the Mach number is further increased. At low Mach numbers the maximum growth rates for the Tanh model are the largest, followed in magnitude by those of the Sutherland and Lock models. At Mach numbers greater than M_* the Lock model has the largest growth rates of the fast supersonic modes while those of the Tanh and Sutherland models are roughly equal. The second group of unstable modes, the slow supersonic modes, appear just below M_*. The growth rate of the most unstable of these modes first increases over a small range of Mach numbers and then decreases, approaching a limiting value at larger values of the Mach number. At this value of β_T the maximum growth rates of these slow supersonic modes are about equal. In all cases, the maximum growth rate approaches a limiting value in this range of Mach numbers.

Similar results for $\beta_T = 1.0$ are shown in Figure 25. In region 1 the growth rates obtained from the Tanh model are significantly larger than those of the other models. The maximum growth rates of these later two models are virtually identical in this region. Because this value of β_T corresponds to the saddle point value for the Tanh profile, we see that the maximum growth rate first decreases as the Mach number approaches M_*, levels off and then begins to increase with increasing Mach number. Since the saddle point values for the other two models are lower than one, their behavior is the same as in the previous case; the maximum growth rate decreases as the Mach number approaches M_* and then levels off for higher Mach numbers. Finally as in the previous case, the second group of unstable modes, those which appear at M_*, have maximum growth rates which are approximately equal and have similar behavior.

The maximum growth rates for $\beta_T = 0.5$ are plotted versus the Mach number in Figure 26. Note the change in scale of the maximum growth rate as β_T is decreased. It is important to realize that $\beta_T = 0.5$ is less than the saddle point value for both the Tanh and Lock models but greater than that for the Sutherland model. Thus for the Tanh and Lock models the maximum growth rate decreases up to M_*, levels off and then increases with increasing Mach number. However, for the Sutherland model the behavior is different because this value of β_T is larger than its saddle point value. Therefore, the variation with Mach number is the same as in the previous two cases. However, if the stationary gas were to be sufficiently cooled, we would expect that the maximum growth rate of the Sutherland model would behave in the same manner as the other two models at higher Mach numbers. Finally, as in the previous two cases, the second group of unstable modes have maximum growth rates which are approximately equal and have similar behavior in this range of Mach numbers.

Further insight into how the choice of thermodynamic model effects the growth rate of the unstable modes is provided by the results shown in Figures 27 and 28. In these figures we show the variation of the growth rate of both the fast and slow unstable supersonic modes for $\beta_T = 2.0$ and M = 2.5 (Figure 27) and M = 5.0 (Figure 28) with the frequency of the disturbance. The results at Mach 2.5 show that the slow unstable supersonic modes exist in a very narrow range of frequencies compared to that of the unstable fast supersonic modes. The shape of the $-\alpha_i$ versus ω curves for the slow modes is similar for all of the models. The widest range of frequencies of the unstable slow supersonic modes and the maximum growth rates are those of the Tanh model, followed by those of the Sutherland model and then the Lock model.

These results are somewhat different for the unstable fast supersonic modes, for which the Lock model has the largest maximum growth rates and the widest range of unstable frequencies. In terms of the maximum growth rates and range of unstable frequencies the Sutherland model is the next largest, followed by the Tanh model. Similar results for Mach 5 are shown in Figure 28. Note the change in scales between these two figures. All of the features shown in the previous figure appear in this figure. The only exception is for the slow supersonic modes in which now the Lock model has a slightly larger growth rate than the Sutherland model.

It is apparent from the results shown in Figure 27 that the curves of growth rate versus frequency for the fast supersonic modes have two local maxima at this value of β_T and Mach number. As the Mach number increases the frequency of the maximum growth rate shifts towards higher frequencies. This is shown in the results of Figure 29, where we show the variation of the growth rate with frequency for β_T = 2.0 and Mach numbers of 2.3, 2.4, and 2.5 for the Sutherland model. The maximum of the growth rate occurs at a value of ω of about 0.05 at Mach 2.3. At Mach 2.4 a second maximum, at an ω of about 0.11 has appeared which is roughly equal to that at 0.04. Finally, at Mach 2.5, the maximum growth rate is at an ω of 0.12. Thus, as the Mach number increases there is a discontinuous jump in the frequency of the maximum growth rate at some Mach number.

The change in the overall maximum growth rate as a function of β_T at fixed Mach number is rather complex. This is due to the fact that for Mach numbers greater than M_* there are now two unstable modes, one in region 2 and another in region 4. An increase in β_T can result in a change in type of the most unstable mode. Some results bearing on this are shown in Figure 30. Here we have plotted the maximum growth rate as a function of β_T for selected values of the Mach number for the three models. For example, at Mach 2 the most unstable mode for the Tanh model is a slow supersonic mode for values of β_T up to 1.25 while it is a subsonic mode for $\beta_T \geq 1.50$. For the Lock profile, again at Mach 2, the most unstable mode is a slow supersonic one up to $\beta_T = 0.75$, a fast supersonic mode at $\beta_T = 1.0$, and subsonic modes at values of β_T greater than or equal to 1.25. Finally, the Sutherland model at the same Mach number has, as its most unstable mode, a slow supersonic one at $\beta_T = 0.5$, a fast supersonic at 0.75, and subsonic modes for β_T greater than or equal to 1.0. This change in mode type is related to the increase in M_* with increasing β_T independently of the thermodynamic model. Thus as β_T is increased the extent of region 1 of the $c_r - M$ diagram increases so that unstable modes at fixed M can undergo a change from supersonic to subsonic.

The general trends of variation of the maximum growth rate with β_T are similar for the Tanh and Lock models. At $M = 1.5$ the maximum growth rate is a monotonically decreasing function of β_T over the range for which we have obtained results. At the other values of the Mach number there is first a decrease in the maximum growth rate with increasing β_T and then a slight increase with a further increase in β_T. The Sutherland model yields somewhat different results. Only at Mach 3 is the variation of the maximum growth rate similar to that obtained from the other two models; a slight decrease followed by a small increase as β_T is increased from 0.5 to 2.0. At Mach 2 the Sutherland model gives a monotonically increasing maximum growth rate with increasing β_T and at Mach 1.5 there is first a small increase followed by a slow decrease as β_T is increased.

4. Conclusions. The characteristic features of the solutions to the stability problem for the compressible mixing layer are qualitatively similar for all of the thermodynamic models used in this study. However,

there are quantitative differences between the results obtained from the different models. These range from about 10% in the phase speeds to, in the most extreme case, about 50% difference in the maximum growth rates.

Despite these quantitative differences there is an underlying similarity in the qualitative behavior of the solutions to the stability problem. For all three thermodynamic models the regularity condition yields a cubic in Mach number at fixed β_T and for a critical value, $\hat{\beta}_T$, there is a saddle point. The behavior of the solutions to the stability problem depends on whether β_T is larger or smaller than $\hat{\beta}_T$. If β_T is larger than $\hat{\beta}_T$ the subsonic modes are transformed into fast supersonic modes at the Mach number at which their phase speed equals that of the sonic wave in the stationary stream. On the other hand, if β_T is smaller than $\hat{\beta}_T$ the subsonic modes are transformed into slow supersonic modes when their phase speed equals the sonic speed of the moving stream. If $\beta_T = \hat{\beta}_T$, then the phase speeds of the subsonic neutral modes are constant. This mode splits into a pair of fast and slow supersonic modes at M_*. For any value of β_T there is a single band of unstable subsonic modes in region1, but there are two bands of unstable supersonic modes, one in region 2 and one in region 4. For all of the thermodynamic models, the second band of unstable supersonic modes appears when the Mach number equals M_*. These second modes are slow supersonic modes if $\beta_T > \hat{\beta}_T$ and fast supersonic modes if $\beta_T < \hat{\beta}_T$. Both the fast and slow unstable supersonic modes have a rather small variation in the phase speed about the mean value.

We have found that, independent of the thermodynamic model, the maximum growth rates of the unstable modes decrease by a factor of 5 to 10 as the Mach number is increased from zero to M_*. As the Mach number is increased beyond M_* the maximum growth rates of the fast supersonic modes approach a limiting value. On the other hand, the maximum growth rates of the slow supersonic modes modes first levels off for $M > M_*$ and then begin to increase with a further increase in the Mach number.

In view of the results presented here we conclude that all of the thermodynamic models yield qualitatively similar results. In view of this, all previous work based on simplified thermodynamic models yields qualitatively correct results. Because of the analytical simplicity of the Tanh model and because it appears to be a reasonable approximation to the mean velocity and temperature profiles we suggest that it is appropiate for use in nonparallel and nonlinear models of the stability of the compressible mixing layer.

REFERENCES

Blumen, W. 1970 Shear Layer Instability of an Inviscid Compressible Fluid. J. Fluid Mech., 40, 769-781.

Blumen, W., Drazin, P. G. & Billings, D. F. 1975 Shear Layer Instability of an Inviscid Compressible Fluid. Part 2. J. Fluid Mech., 71, 305-316.

Brown, W. B. 1962 Exact numerical solutions of the complete linearized equations for the stability of compressible boundary layers. Norair Rep. No. NOR-62-15, Northrop Aircraft Inc., Hawthorne, CA.

Chapman, D. R. 1950 Laminar mixing of a compressible fluid. NACA Rep. 958.

Drazin, P. G. & Davey, A. 1977 Shear Layer Instability of an Inviscid Compressible Fluid. Part 3. J. Fluid Mech., 82, 255-260.

Dunn, D. W. & Lin, C. C. 1955 On the stability of the laminar boundary in a compressible fluid. J. Aero. Sci. 22, 455-477.

Gill, A. E. 1965 Instabilities of "Top-Hat" Jets and Wakes in Compressible Fluids. Phys. Fluids, 8, 1428-1430.

Gropengiesser, H. 1969 On the Stability of Free Shear Layers in Compressible Flows. (in German), Deutsche Luft. und Raumfahrt, FB 69-25, 123 pp. Also, NASA Tech. Translation NASA TT F-12,786.

Jackson, T. L. & Grosch, C. E. 1988 Inviscid Spatial Stability of a Compressible Mixing Layer. J. Fluid Mech., in press.

Jackson, T. L. & Grosch, C. E. 1989 Inviscid Spatial Stability of a Compressible Mixing Layer. Part II. The Flame Sheet Model. ICASE Rep. No. 89-18. Also, J. Fluid Mech., submitted.

Klemp, J. B. & Acrivos, A. 1972 A note on the laminar mixing of two uniform parallel semi-infinite streams. J. Fluid Mech., 55, 25-30.

Lees, L. & Lin, C. C. 1946 Investigation of the stability of the laminar boundary layer in a compressible fluid. NACA Tech. Note 1115.

Lees, L. & Reshotko, E. 1962 Stability of the compressible laminar boundary layer. J. Fluid Mech., 12, 555-590.

Lessen, M., Fox, J. A. & Zien, H. M. 1965 On the Inviscid Stability of the Laminar Mixing of Two Parallel Streams of a Compressible Fluid. J. Fluid Mech., 23, 355-367.

Lessen, M., Fox, J. A. & Zien, H. M. 1966 Stability of the Laminar Mixing of two Parallel Streams with Respect to Supersonic Disturbances. J. Fluid Mech., 25, 737-742.

Lock, R. C. 1951 The velocity distribution in the laminar boundary layer between parallel streams. Quart. J. Mech. and Appl. Math., 4, 42-63.

Macaraeg, M. G., Streett, C. L., & Hussaini, M. Y. 1988 A spectral collocation solution to the compressible stability eigenvalue problem. NASA Technical Paper 2858.

Mack, L. M. 1965 Computation of the Stability of the Laminar Compressible Boundary Layer. In *Methods in Computational Physics*. B. Alder, S. Fernbach, and M. Rotenberg, eds. Vol. 4, 247-299, Academic Press.

Mack, L. M. 1984 Boundary layer linear stability theory. In *Special Course on Stability* and *Transition of Laminar Flow*. AGARD Report R-709, 3-1 to 3-81.

Mack, L. M. 1987 Review of linear compressible stability theory. In *Stability of Time Dependent* and *Spatially Varying Flows*. D. L. Dwoyer and M. Y. Hussaini, eds. Springer-Verlag, 164-187.

Mack, L. M. 1989 On the inviscid acoustic-mode instability of supersonic shear flows. Fourth Symposium on Numerical and Physical Aspects of Aerodynamic Flows, California State University, Long Beach, California.

Ragab, S. A. & Wu, J. L. 1988 Instabilities in the Free Shear Layer Formed by Two Supersonic Streams. AIAA Paper 88-0038.

Stewartson, K. 1964 *The Theory of Laminar Boundary Layers in Compressible Fluids*. Oxford University Press, Great Britain.

Tam, C. K. W. & Hu, F. Q. 1988 Instabilities of Supersonic Mixing Layers Inside a Rectangular Channel. AIAA Paper 88-3675.

Ting, L. 1959 On the mixing of two parallel streams. J. Math. Phys., 28, 153-165.

Zhuang, M., Kubota, T. & Dimotakis, P. E. 1988 On the Instability of Inviscid, Compressible Free Shear Layers. AIAA Paper 88-3538.

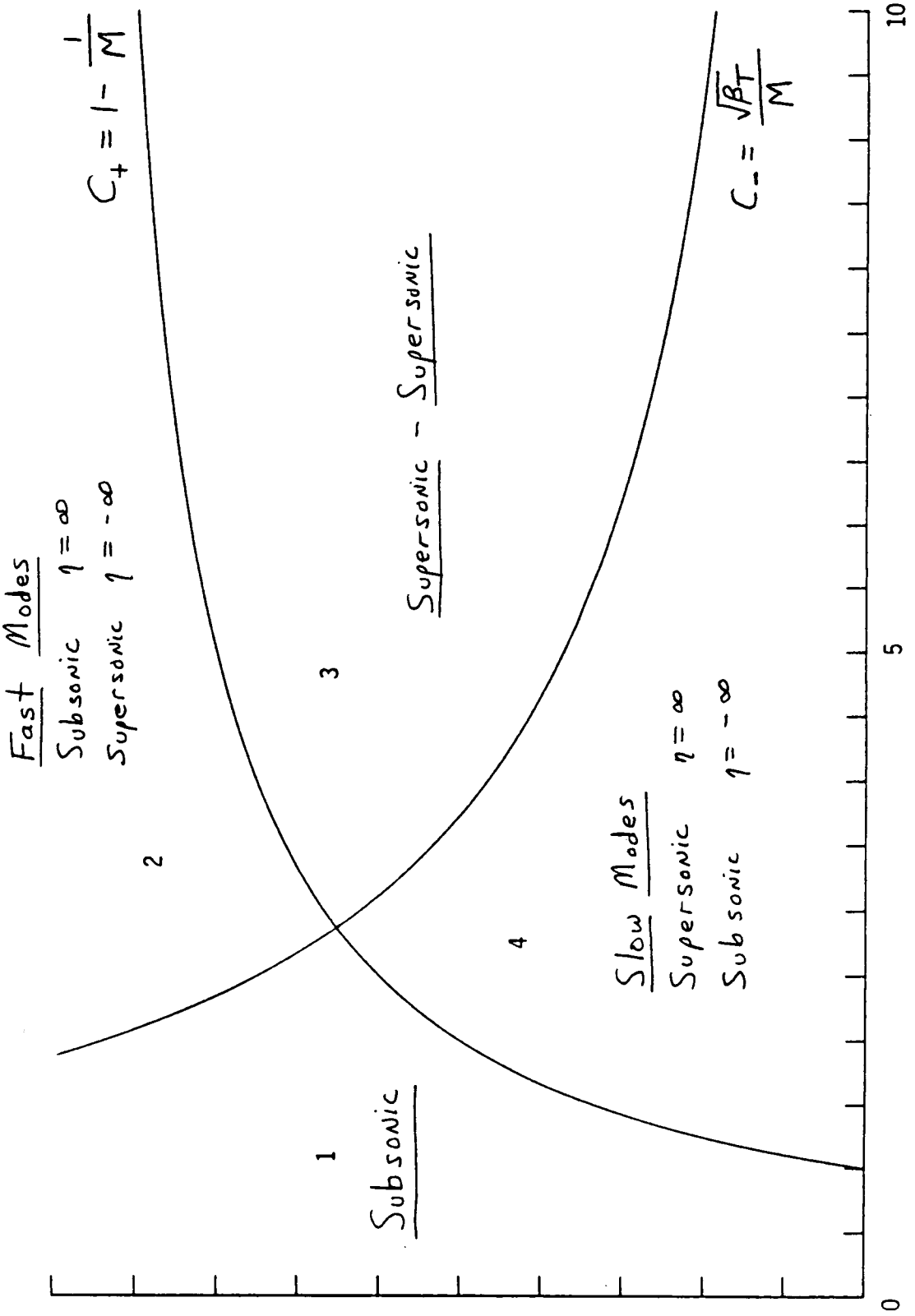

Figure 1. Plots of the sonic speeds $c_\pm$ versus Mach number for $\beta_T = 3.5$.

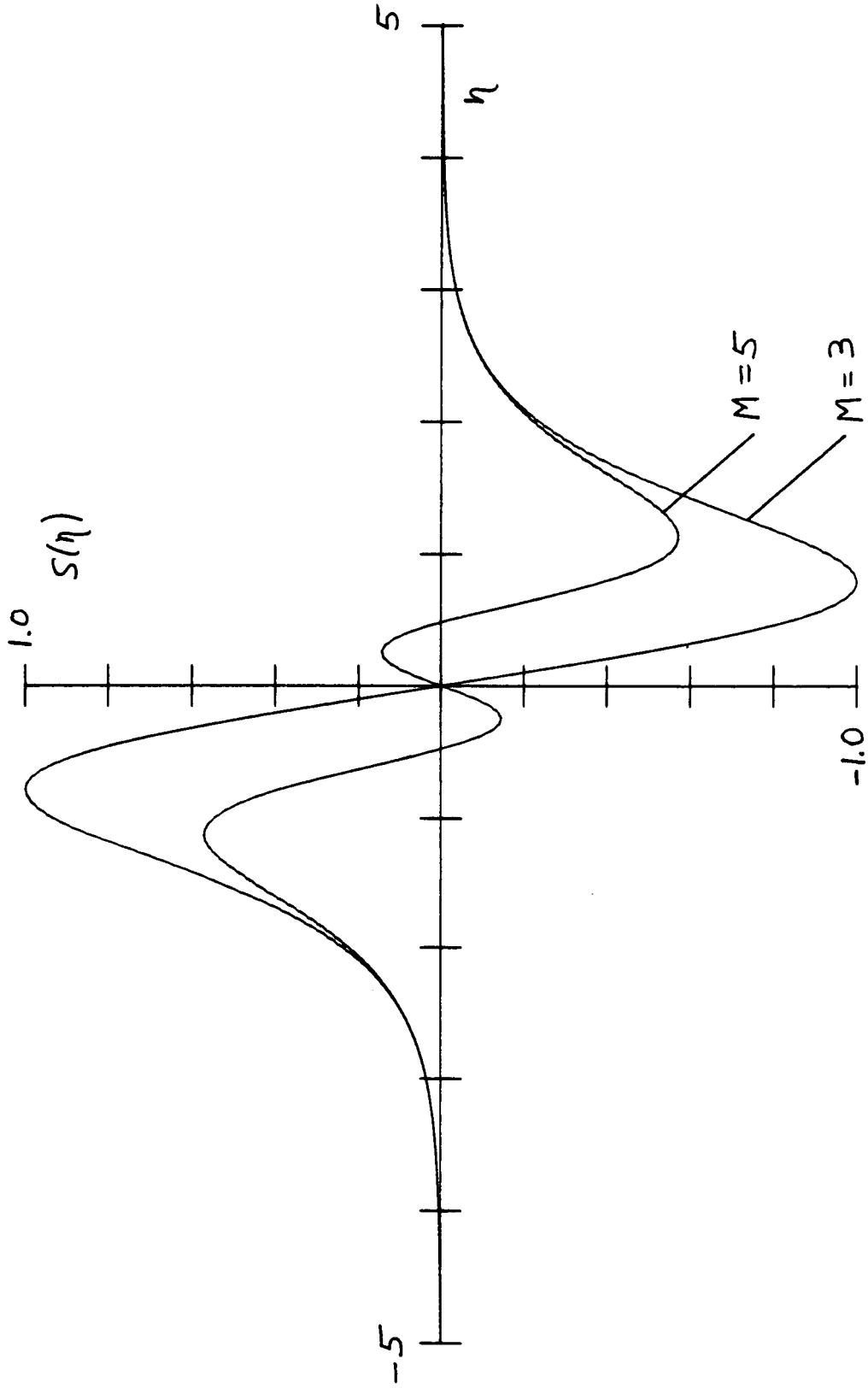

Figure 2. Plot of $S(\eta)$ for $\beta_T = 1.0$ and for $M = 3$ and 5 for the Tanh model.

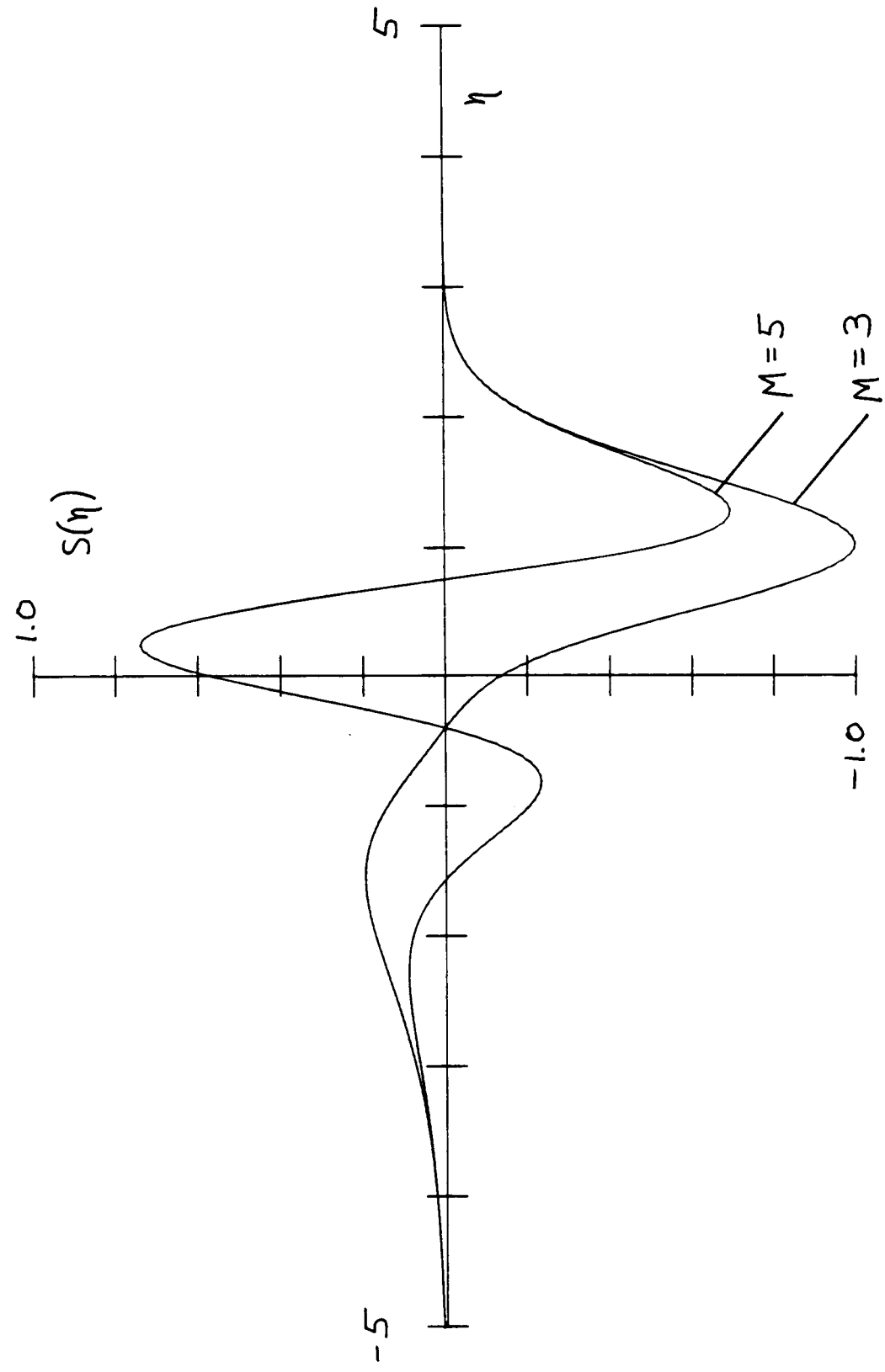

Figure 3. Plot of $S(\eta)$ for $\beta_T = 0.57753$ and for M = 3 and 5 for the Lock model.

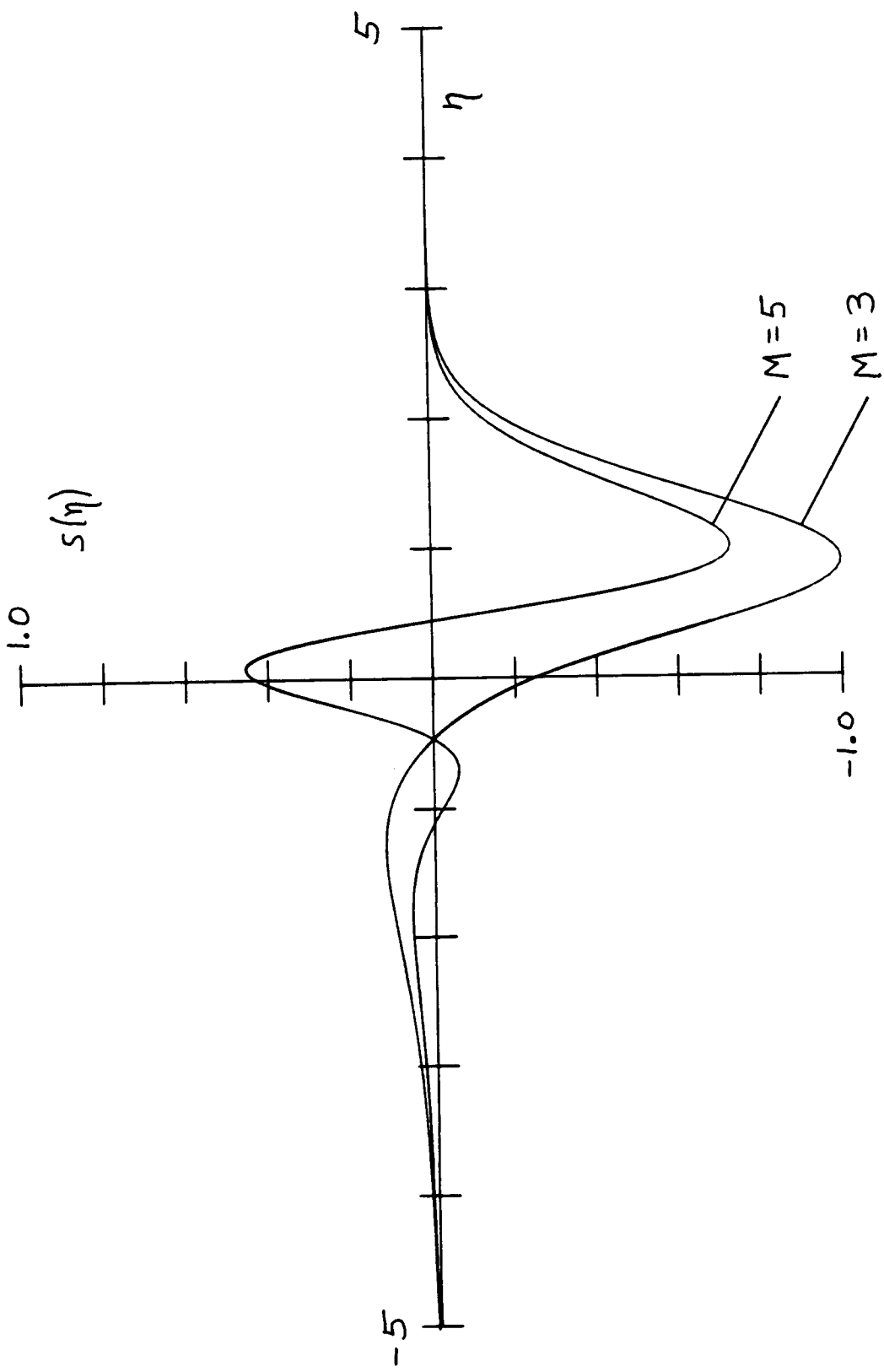

Figure 4. Plot of $S(\eta)$ for β_T = 0.445, Pr = 1, and for M = 3 and 5 for the Sutherland model.

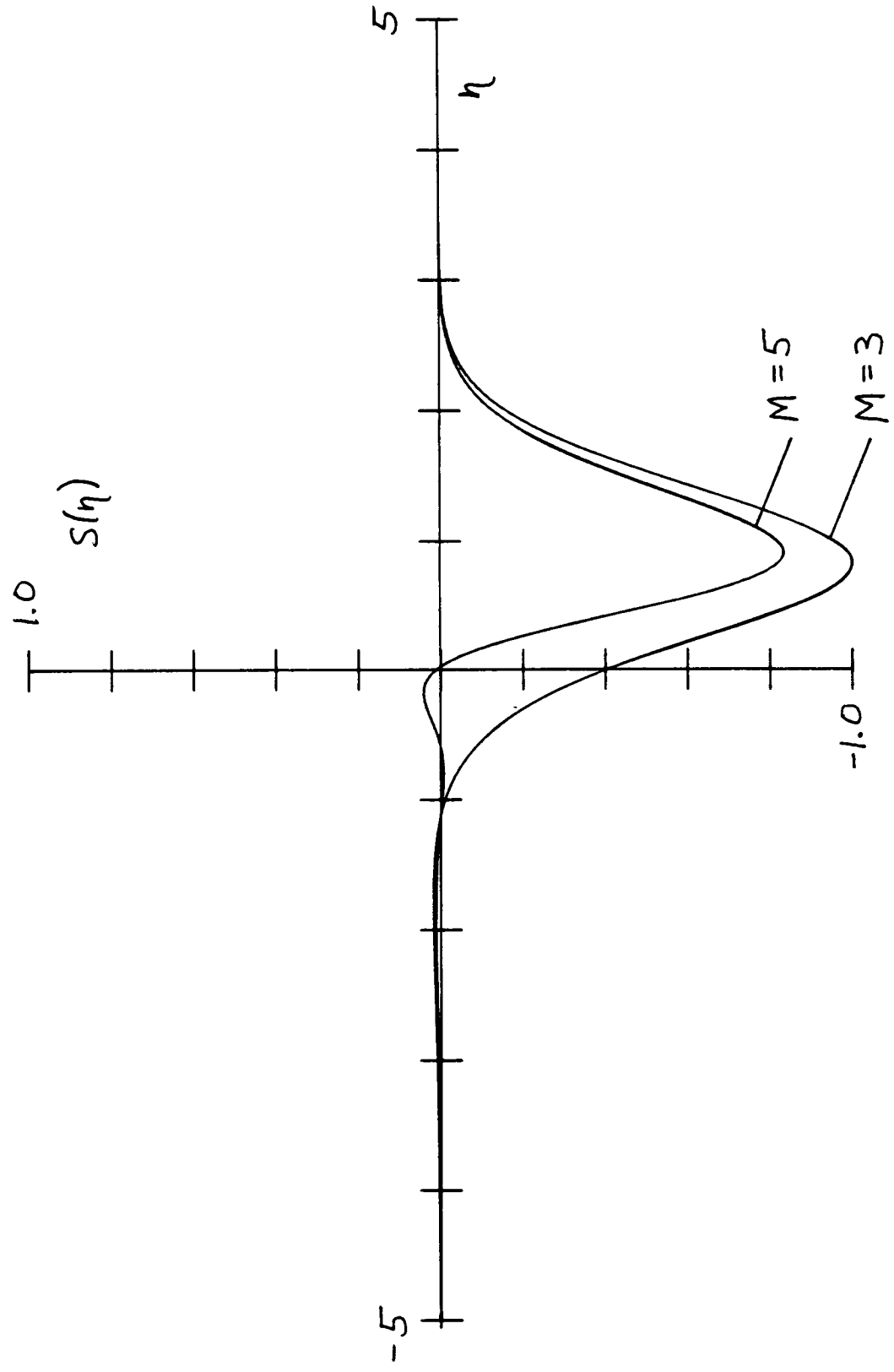

Figure 5. Plot of $S(\eta)$ for $\beta_T = 0.145$, Pr = 0.7, and for M = 3 and 5 for the Sutherland model.

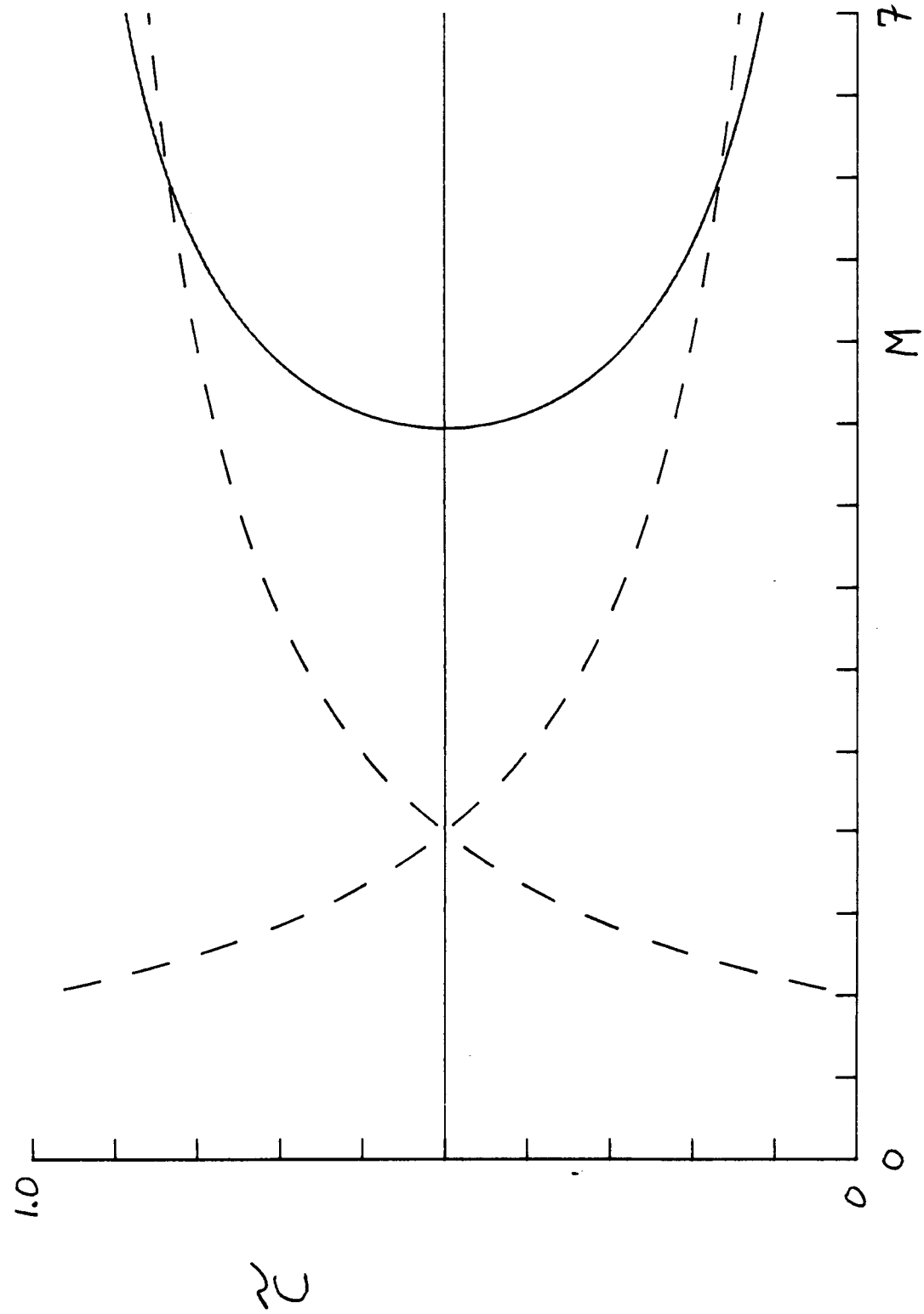

Figure 6. Plot of the real roots of S, ζ (solid curve), versus Mach number for $\beta_T = 1.0$ for the Tanh model. Sonic curves, $c_\pm$ (dashed curves), are also shown.

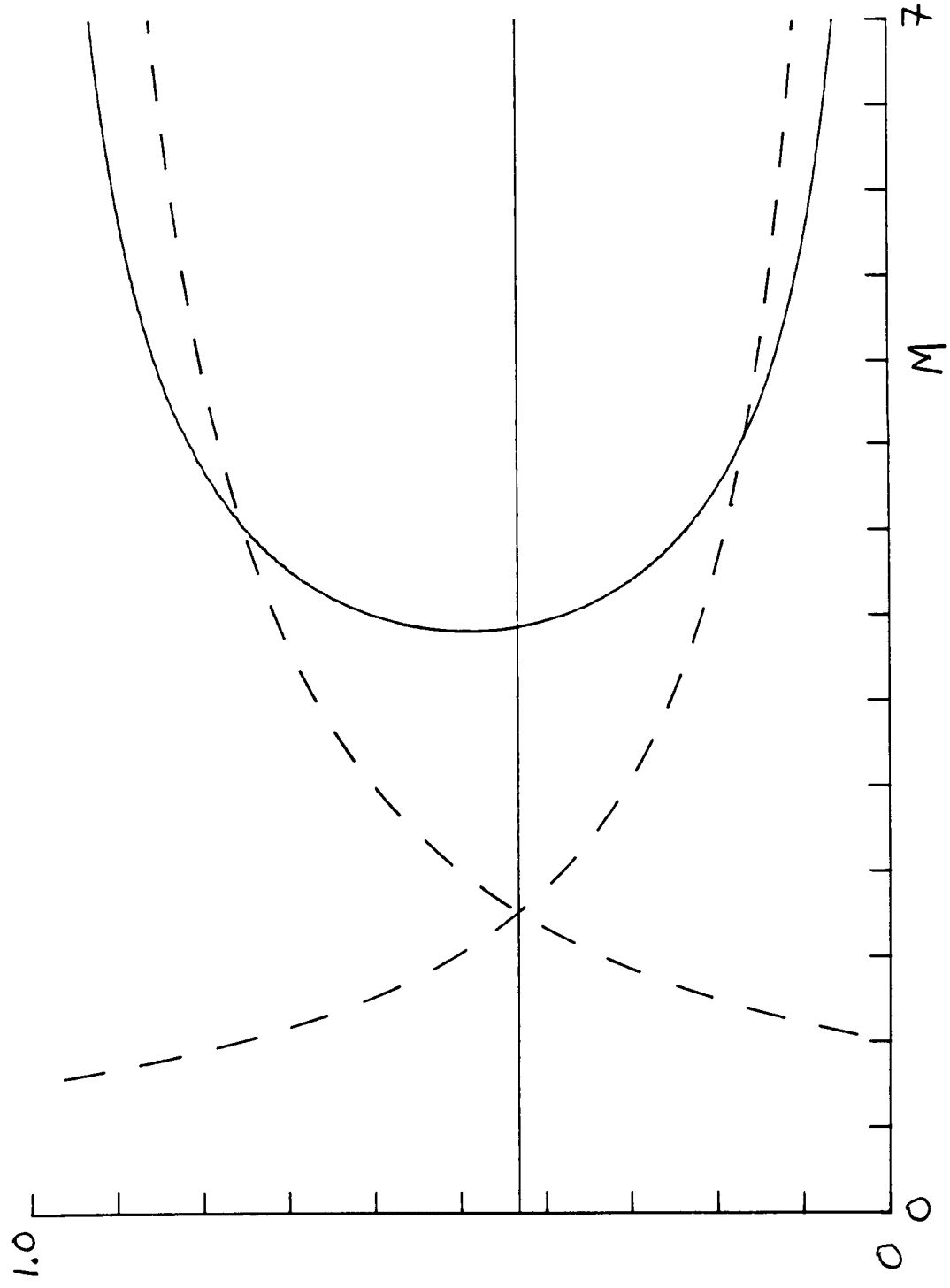

Figure 7. Plot of the real roots of S, ξ (solid curve), versus Mach number for $\beta_T = 0.57753$ for the Lock model. Sonic curves, $c_\pm$ (dashed curves), are also shown.

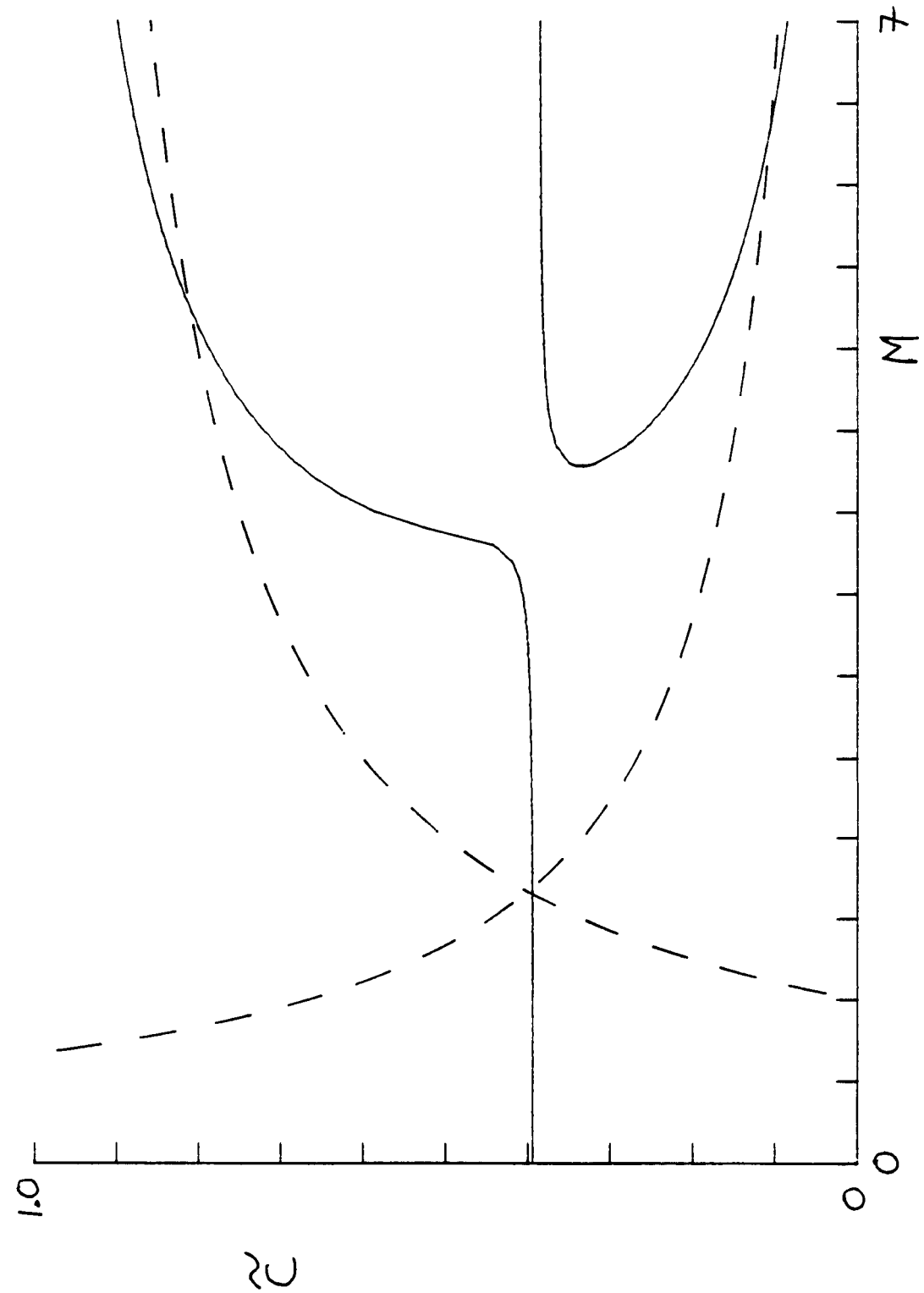

Figure 8. Plot of the real roots of S, $\bar{c}$ (solid curve), versus Mach number for $\beta_T = 0.445$ and Pr = 1.0 for the Sutherland model. Sonic curves, $c_\pm$ (dashed curves), are also shown.

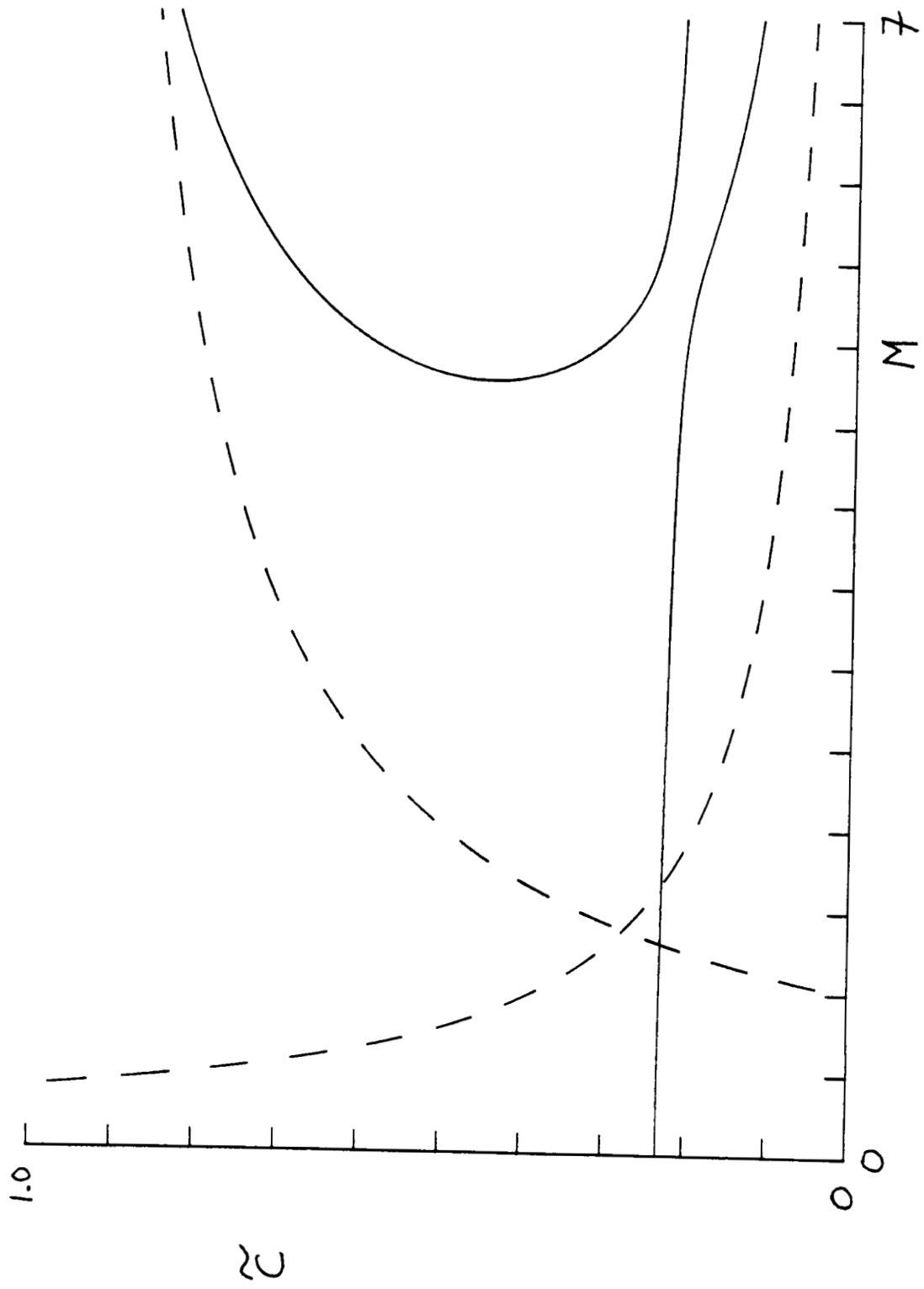

Figure 9. Plot of the real roots of S, $\bar{c}$ (solid curve), versus Mach number for $\beta_T = 0.145$ and $Pr = 0.7$ for the Sutherland model. Sonic curves, $c_\pm$ (dashed curves), are also shown.

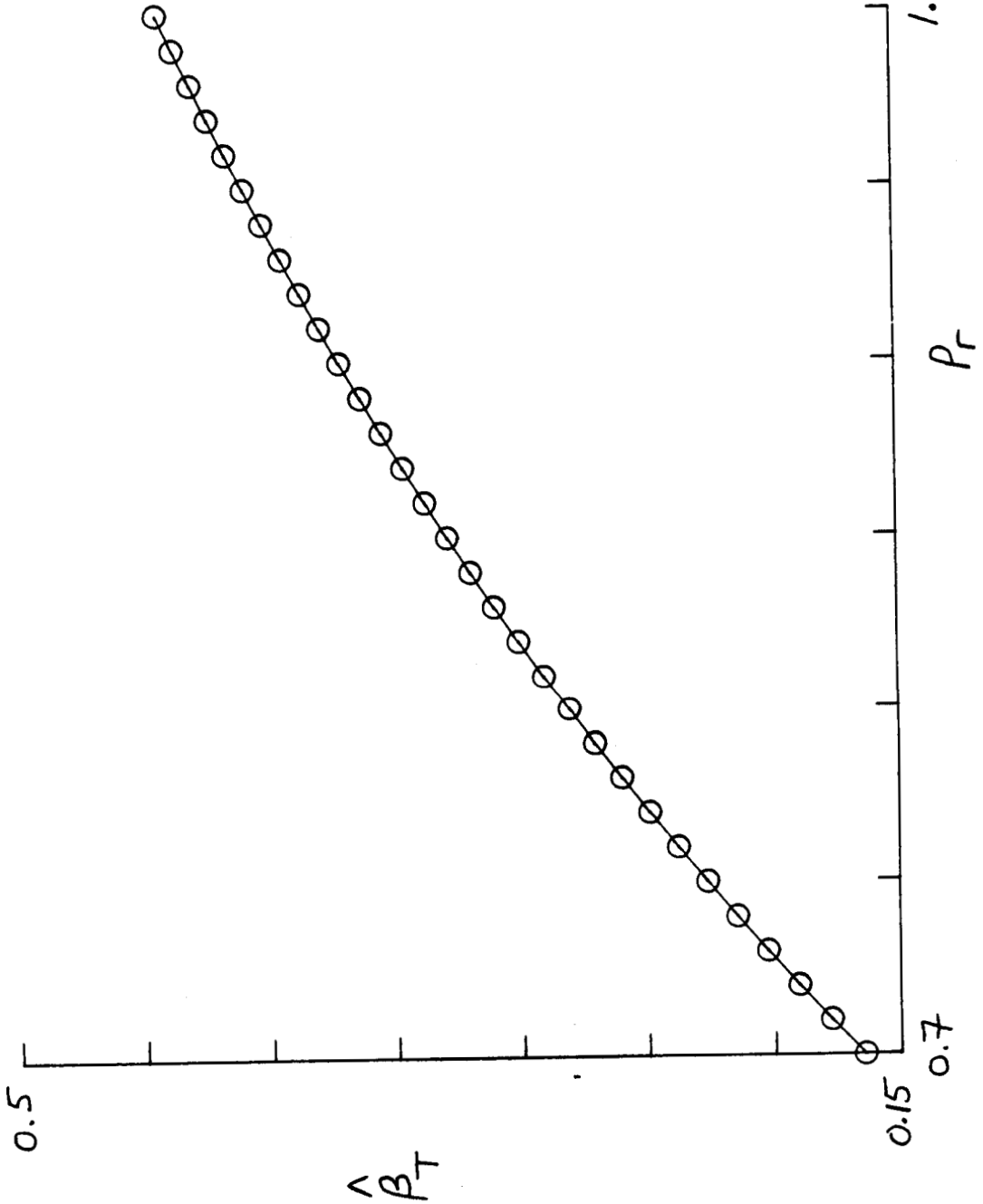

Figure 10. Plot of β_T versus Prandtl number for the Sutherland model.

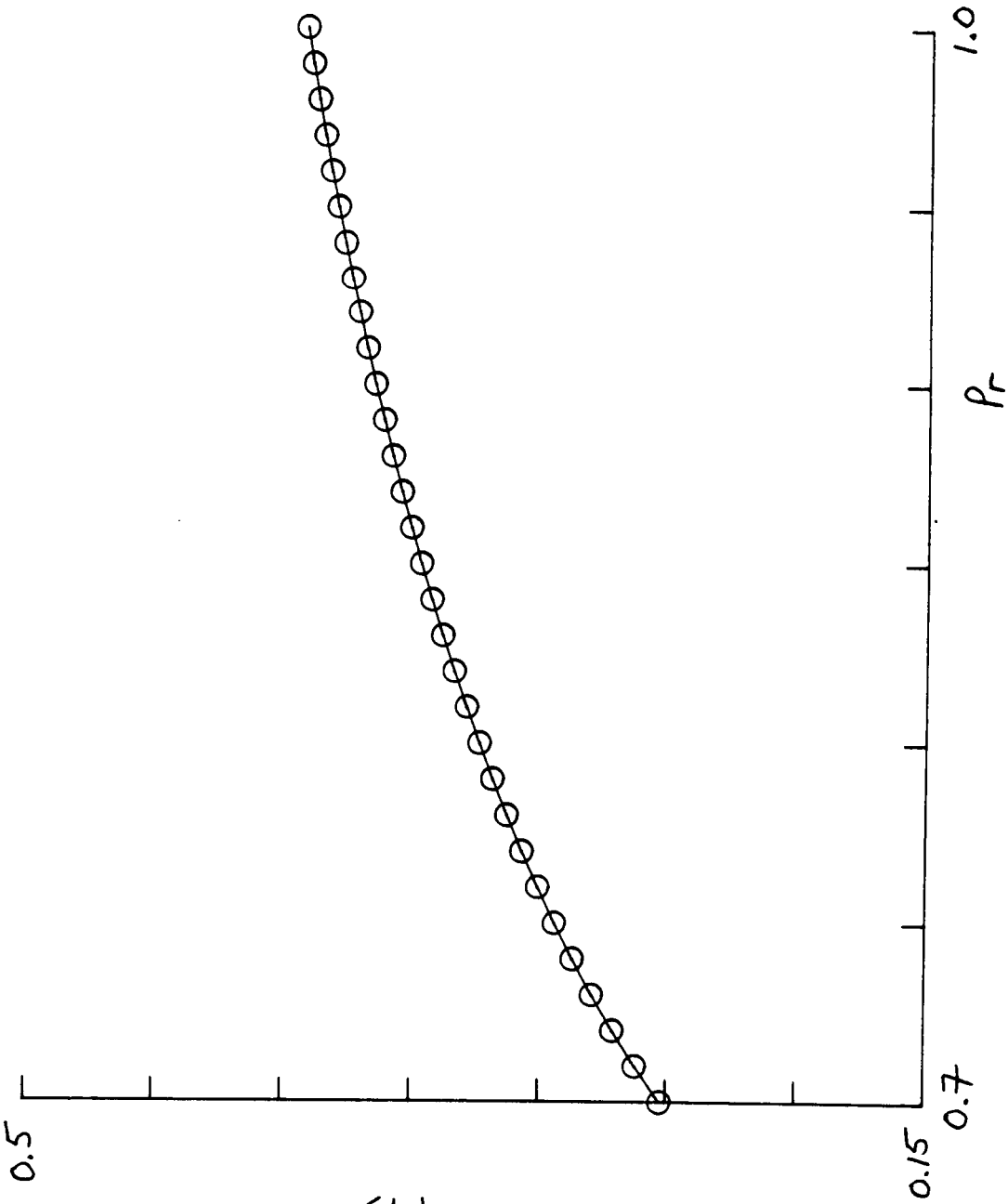

Figure 11. Plot of $\hat{c}$ versus Prandtl number for the Sutherland model.

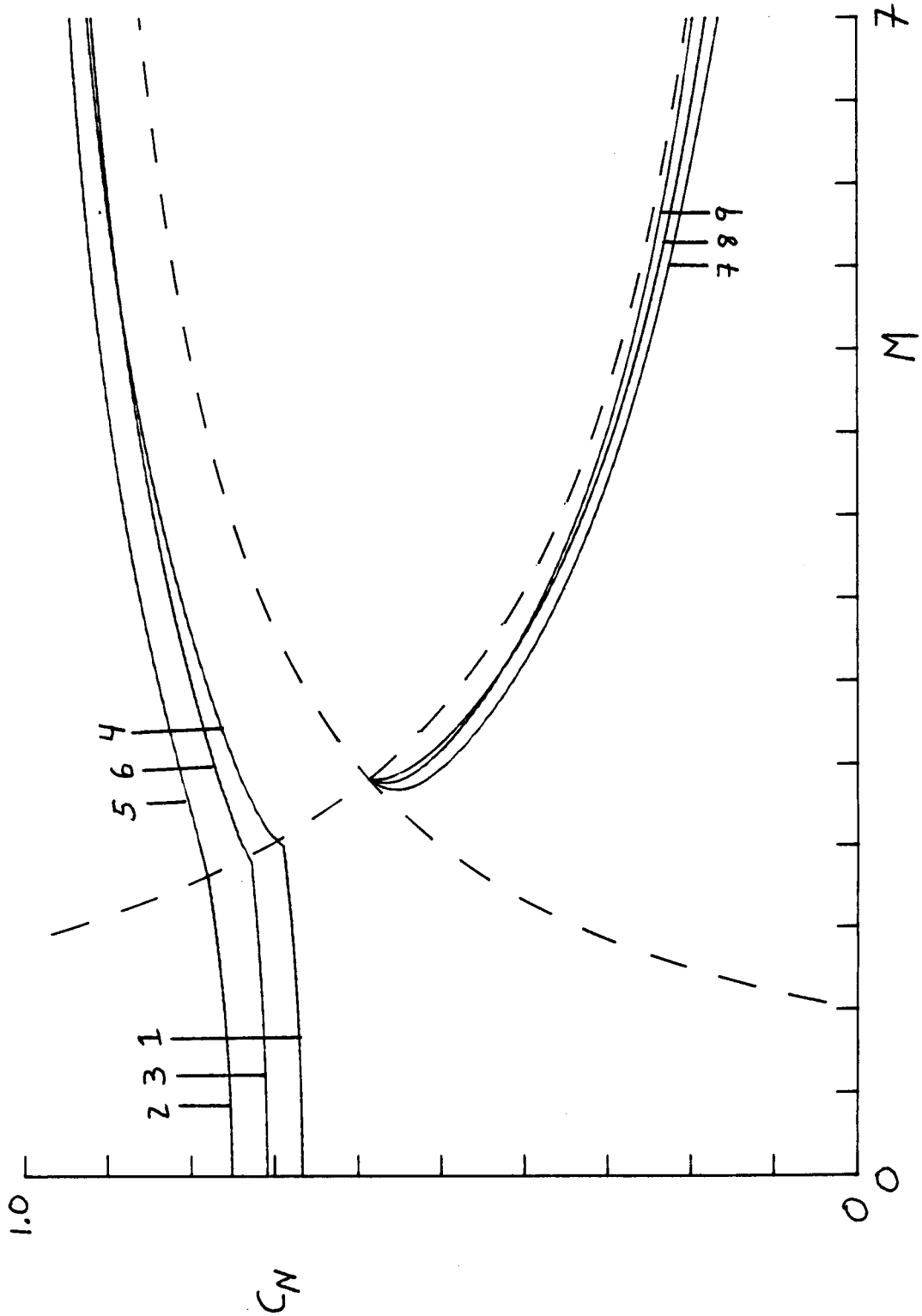

Figure 12. Plots of two dimensional neutral curves for $\beta_T = 2.0$ versus Mach number: phase (solid) and sonic (dashed) speeds; Subsonic Modes: (1) Tanh, (2) Lock, (3) Sutherland; Fast Modes: (4) Tanh, (5) Lock, (6) Sutherland; Slow Modes: (7) Tanh, (8) Lock, (9) Sutherland.

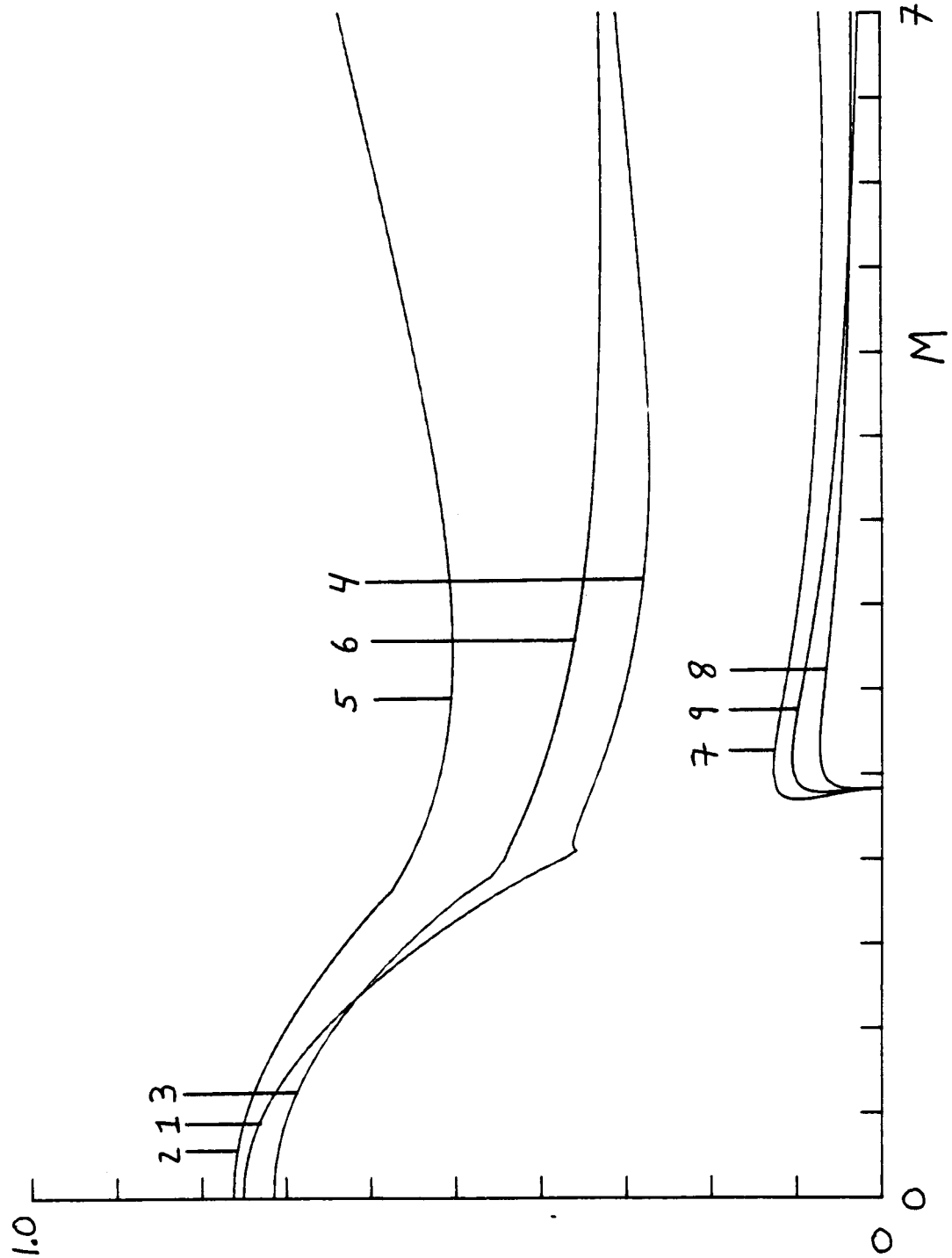

Figure 13. Plots of two dimensional neutral wavenumbers for β_T = 2.0 versus Mach number; Subsonic Modes: (1) Tanh, (2) Lock, (3) Sutherland; Fast Modes: (4) Tanh, (5) Lock, (6) Sutherland; Slow Modes: (7) Tanh, (8) Lock, (9) Sutherland.

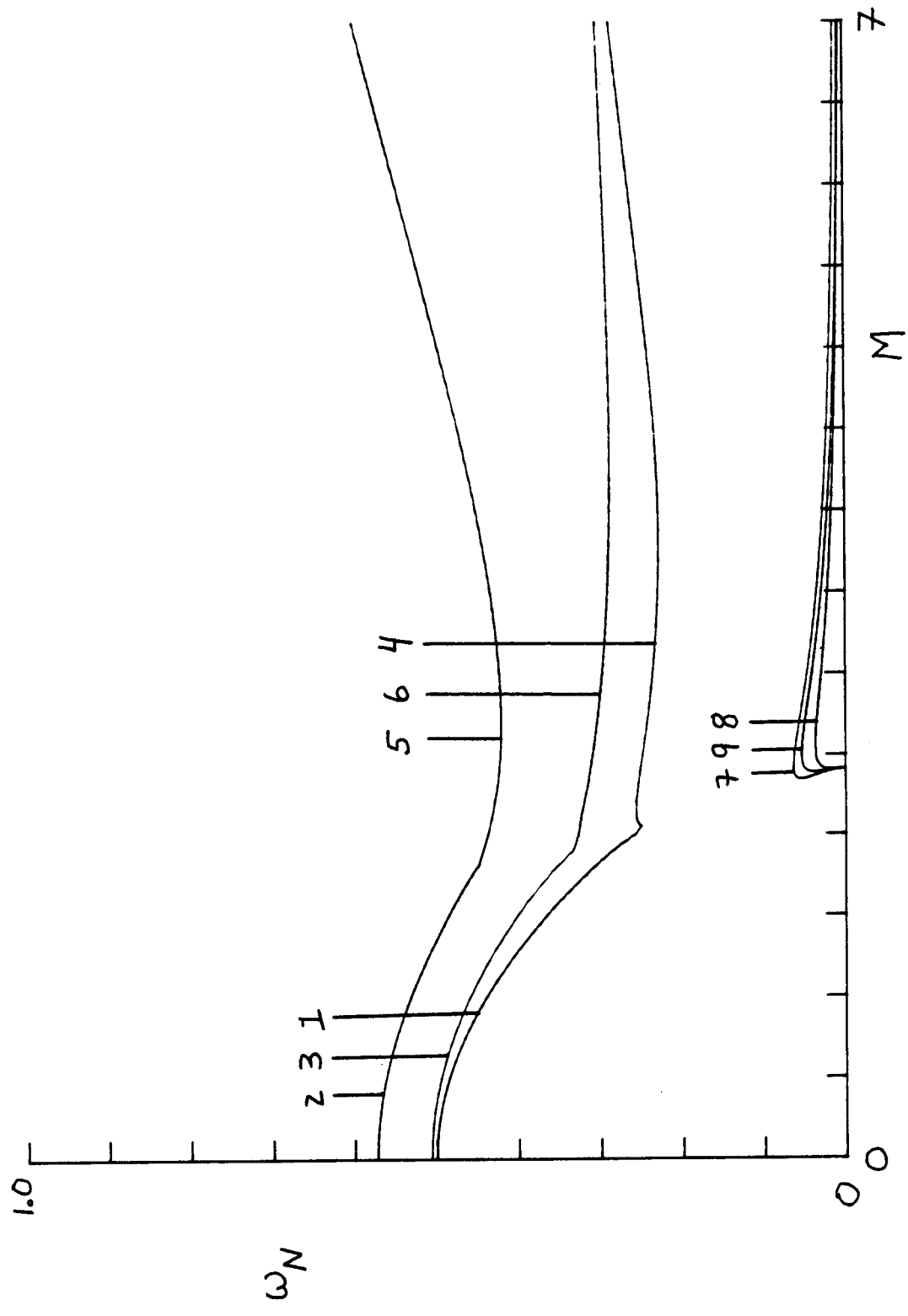

Figure 14. Plots of two dimensional neutral frequencies for β_T = 2.0 versus Mach number; Subsonic Modes: (1) Tanh, (2) Lock, (3) Sutherland; Fast Modes: (4) Tanh, (5) Lock, (6) Sutherland; Slow Modes: (7) Tanh, (8) Lock, (9) Sutherland.

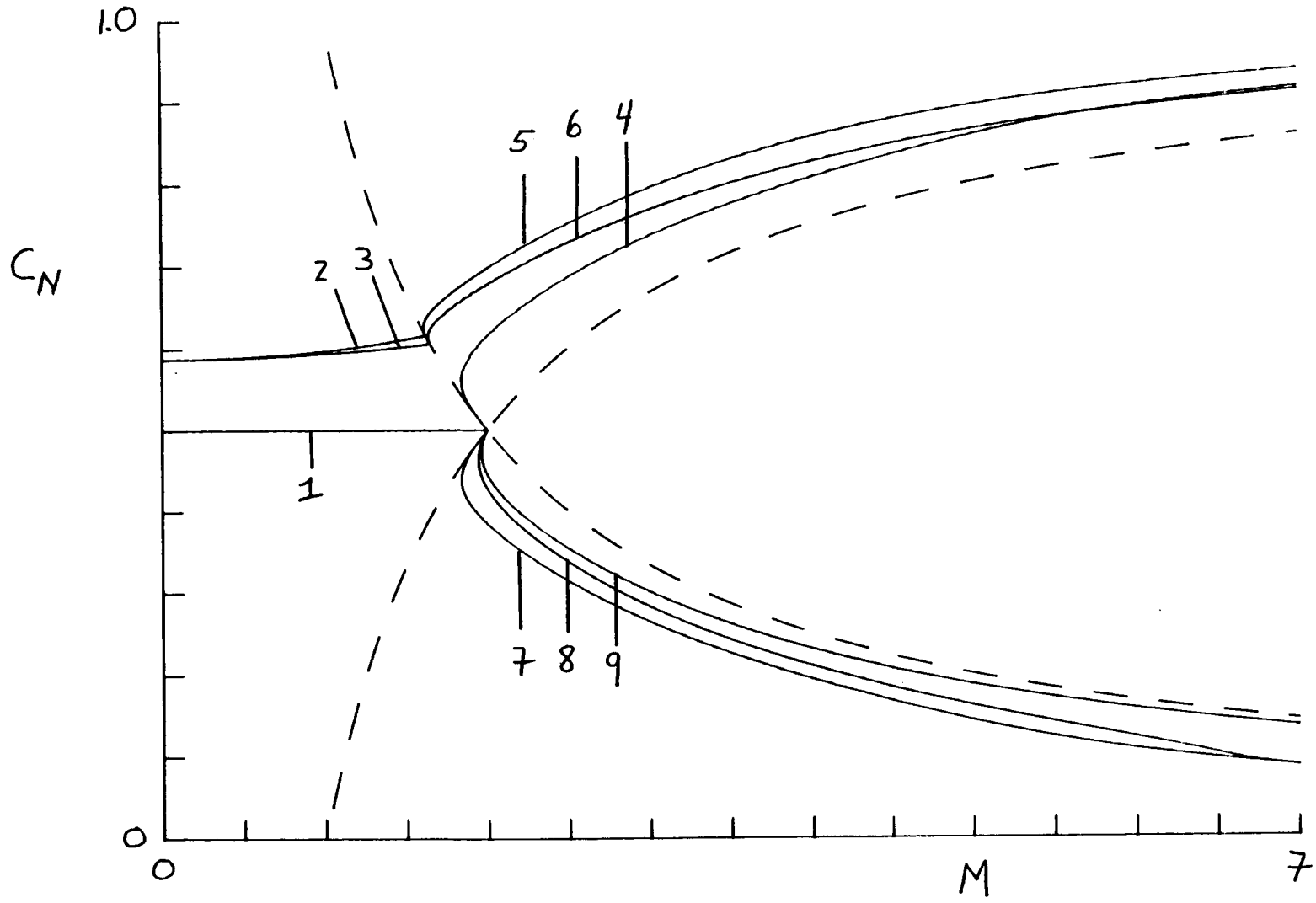

Figure 15. Plots of two dimensional neutral curves for β_T = 1.0 versus Mach number: phase (solid) and sonic (dashed) speeds; Subsonic Modes: (1) Tanh, (2) Lock, (3) Sutherland; Fast Modes: (4) Tanh, (5) Lock, (6) Sutherland; Slow Modes: (7) Tanh, (8) Lock, (9) Sutherland.

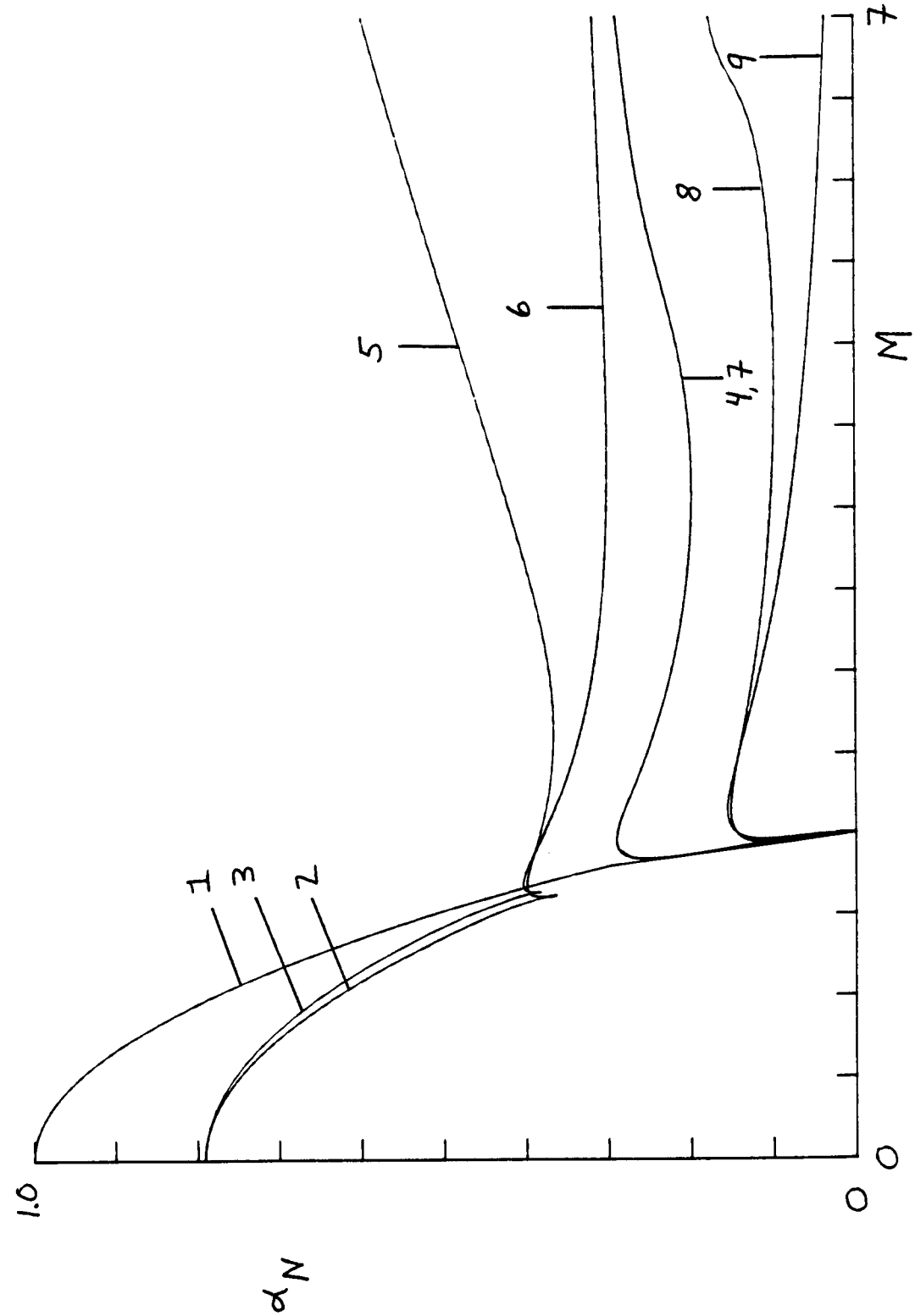

Figure 16. Plots of two dimensional neutral wavenumbers for $\beta_T = 1.0$ versus Mach number; Subsonic Modes: (1) Tanh, (2) Lock, (3) Sutherland; Fast Modes: (4) Tanh, (5) Lock, (6) Sutherland; Slow Modes: (7) Tanh, (8) Lock, (9) Sutherland.

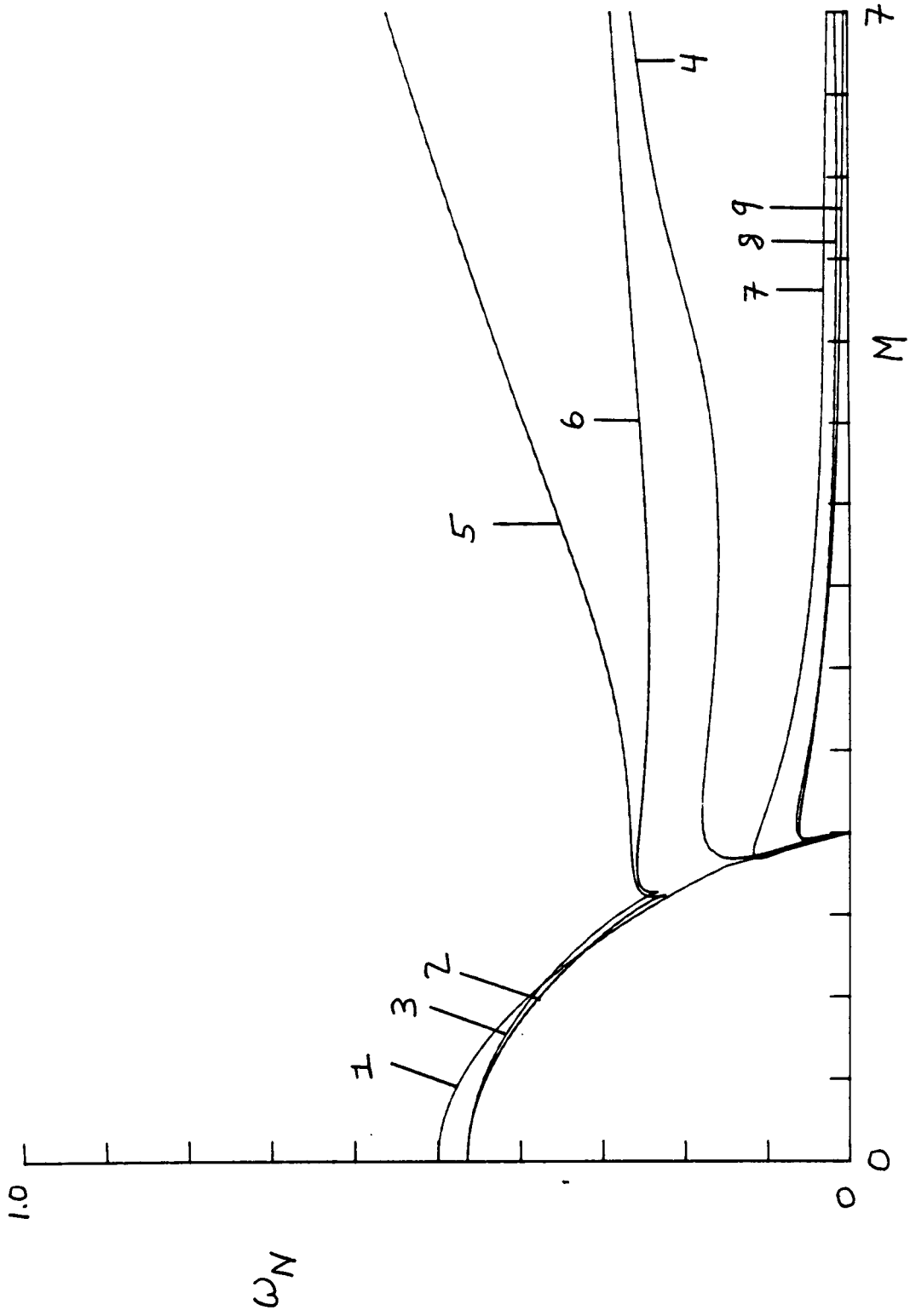

Figure 17. Plots of two dimensional neutral frequencies for β_T = 1.0 versus Mach number; Subsonic Modes: (1) Tanh, (2) Lock, (3) Sutherland; Fast Modes: (4) Tanh, (5) Lock, (6) Sutherland; Slow Modes: (7) Tanh, (8) Lock, (9) Sutherland.

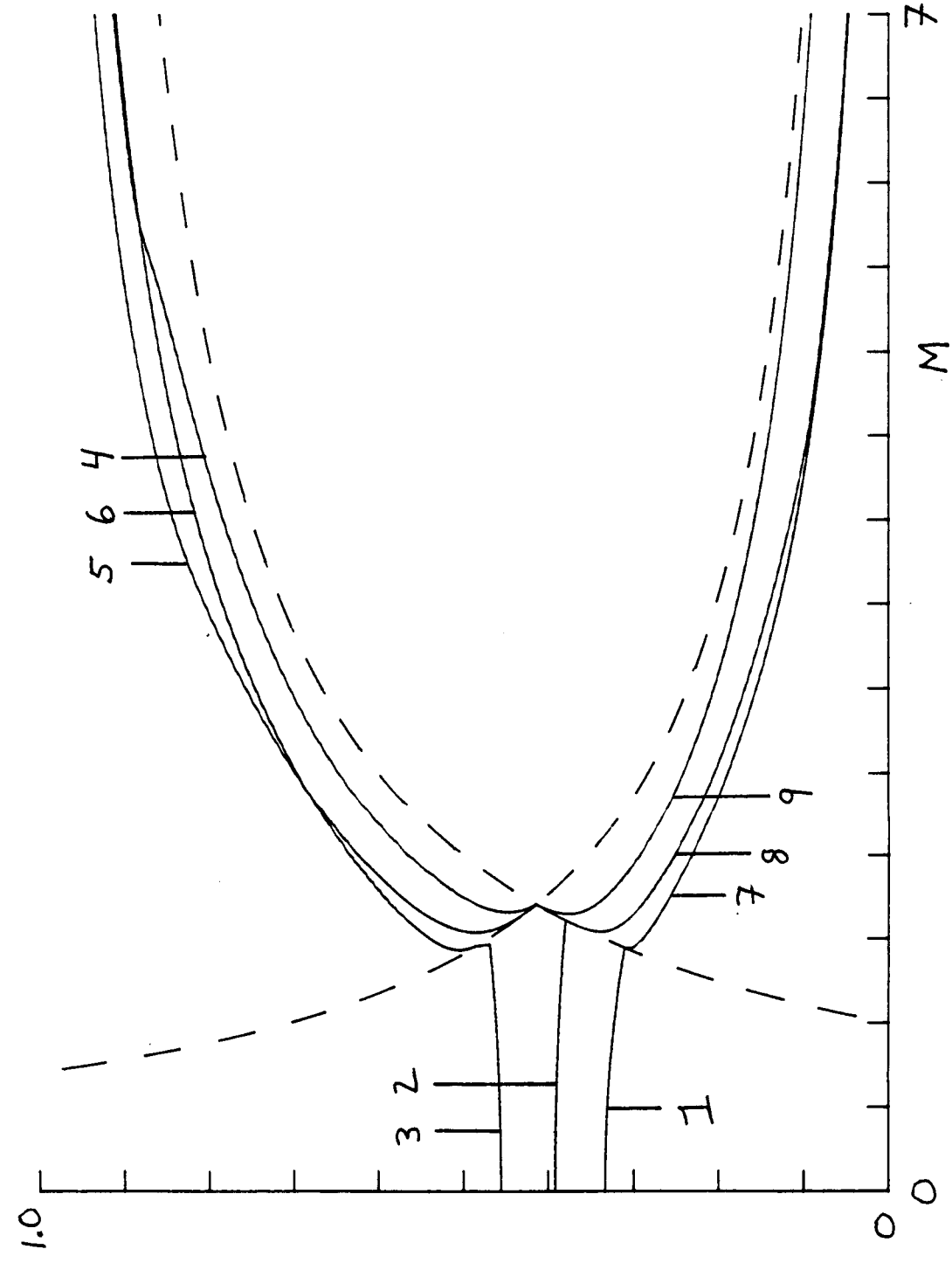

Figure 18. Plots of two dimensional neutral curves for $\beta_T = 0.5$ versus Mach number: phase (solid) and sonic (dashed) speeds; Subsonic Modes: (1) Tanh, (2) Lock, (3) Sutherland; Fast Modes: (4) Tanh, (5) Lock, (6) Sutherland; Slow Modes: (7) Tanh, (8) Lock, (9) Sutherland.

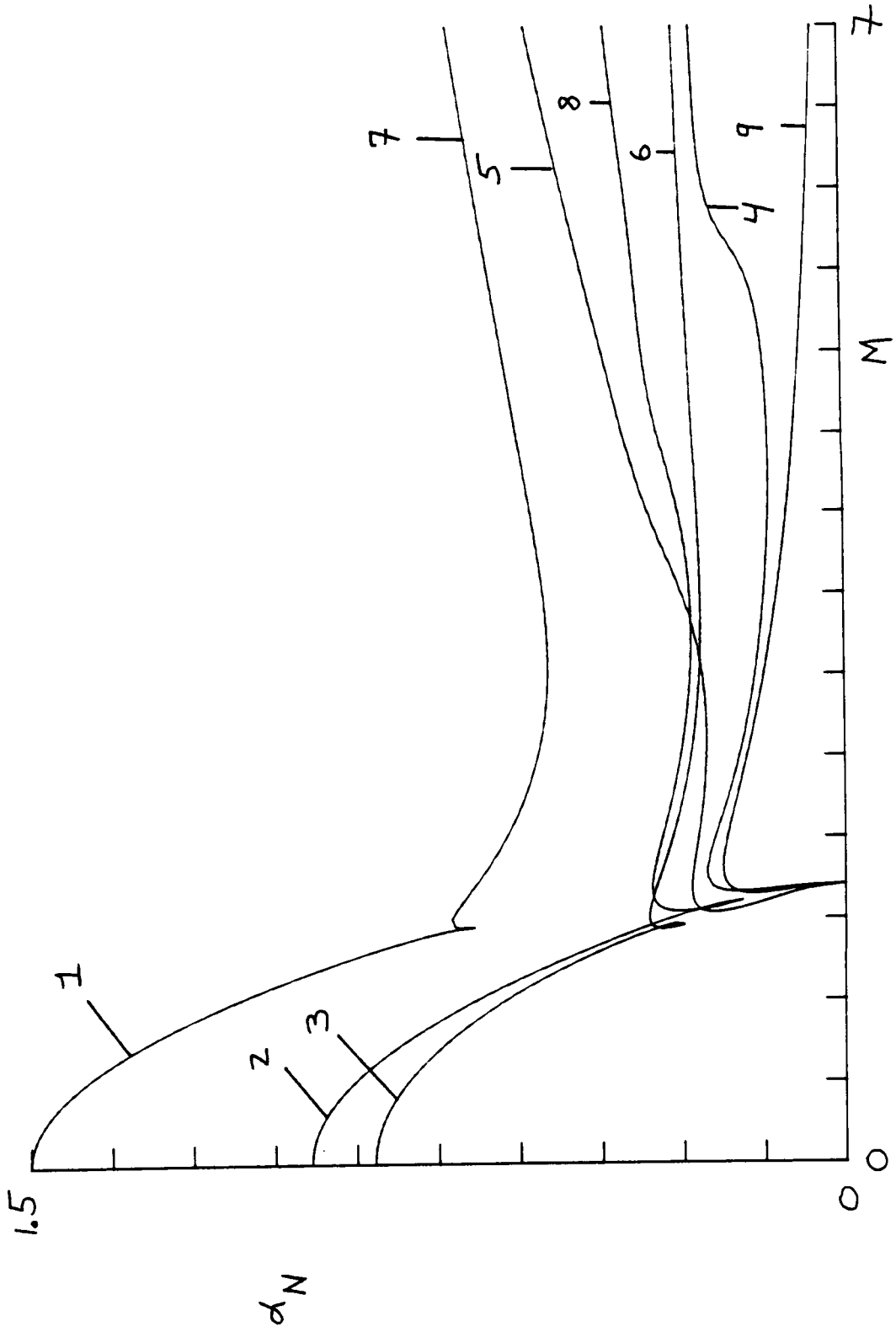

Figure 19. Plots of two dimensional neutral wavenumbers for β_T = 0.5 versus Mach number; Subsonic Modes: (1) Tanh, (2) Lock, (3) Sutherland; Fast Modes: (4) Tanh, (5) Lock, (6) Sutherland; Slow Modes: (7) Tanh, (8) Lock, (9) Sutherland.

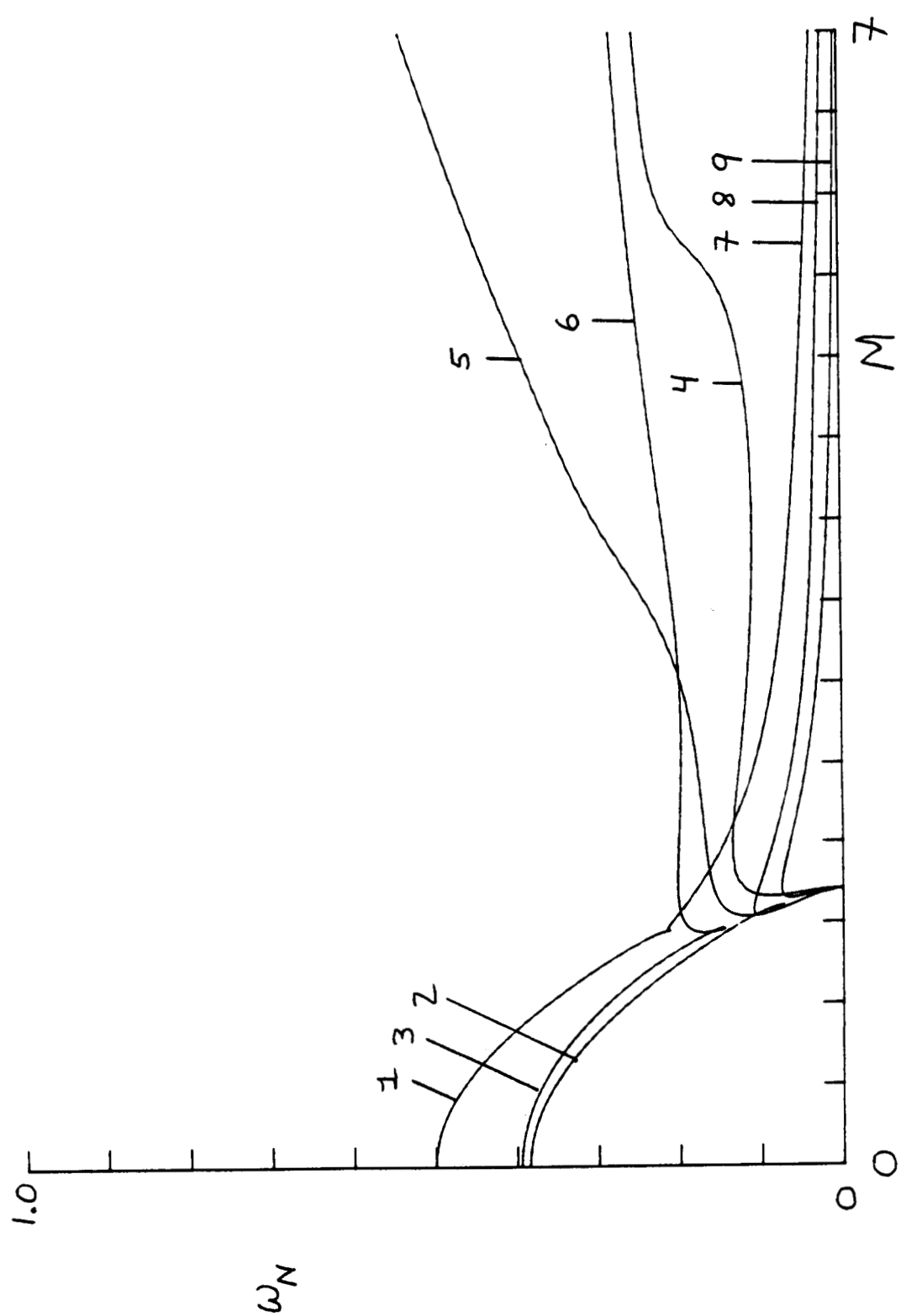

Figure 20. Plots of two dimensional neutral frequencies for $\beta_T = 0.5$ versus Mach number; Subsonic Modes: (1) Tanh, (2) Lock, (3) Sutherland; Fast Modes: (4) Tanh, (5) Lock, (6) Sutherland; Slow Modes: (7) Tanh, (8) Lock, (9) Sutherland.

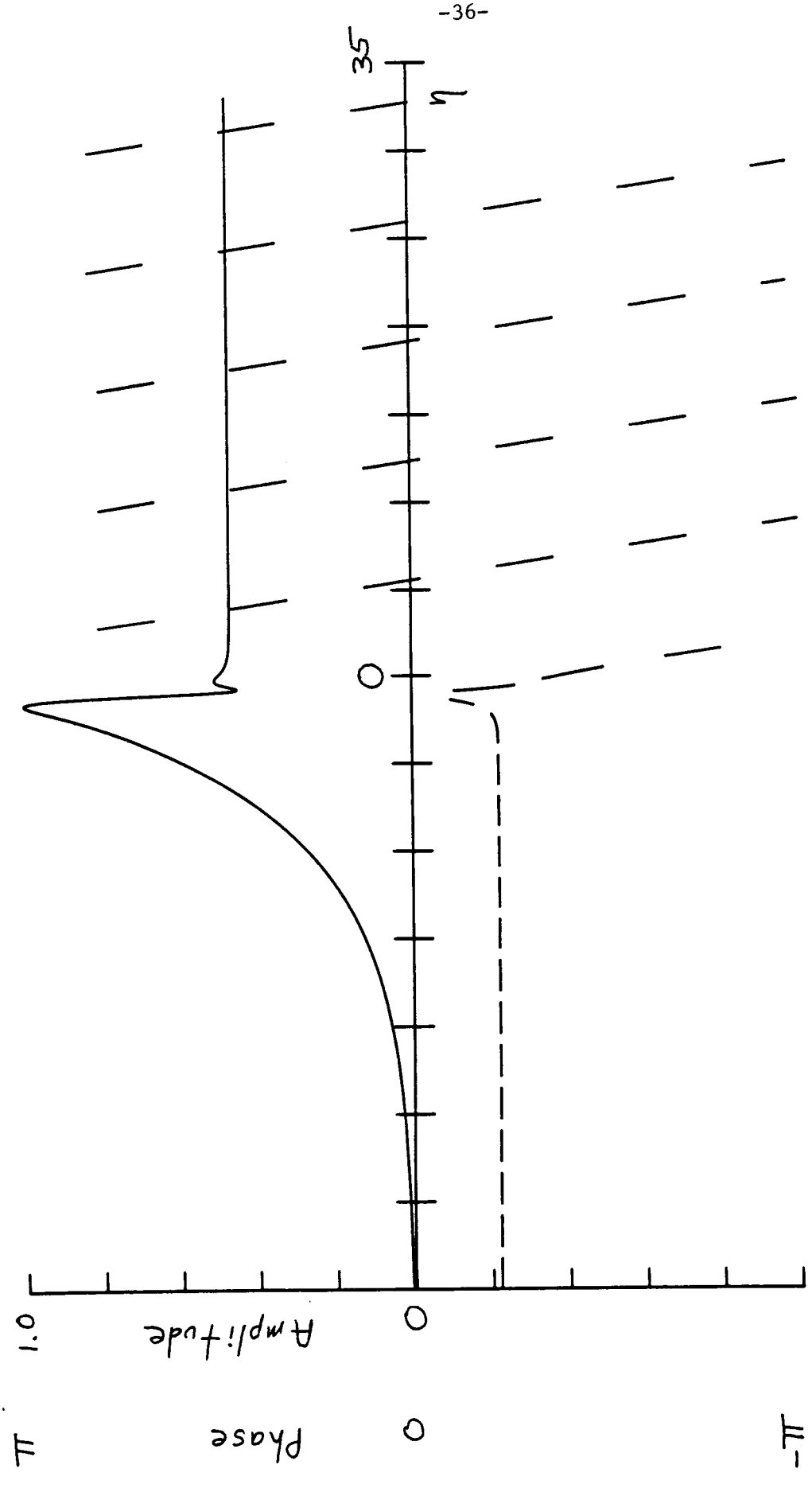

Figure 21. Plot of the two dimensional slow supersonic neutral eigenfunction $\Pi(\eta)$ along the contour $\eta = \eta_r - i$. The solid curve corresponds to the amplitude and the dashed curve to the phase. $M = 5$, $\beta_T = 1$: Tanh Model; $\omega_N = 0.030847$, $\alpha_N = 0.215661$, $c_N = 0.143030$.

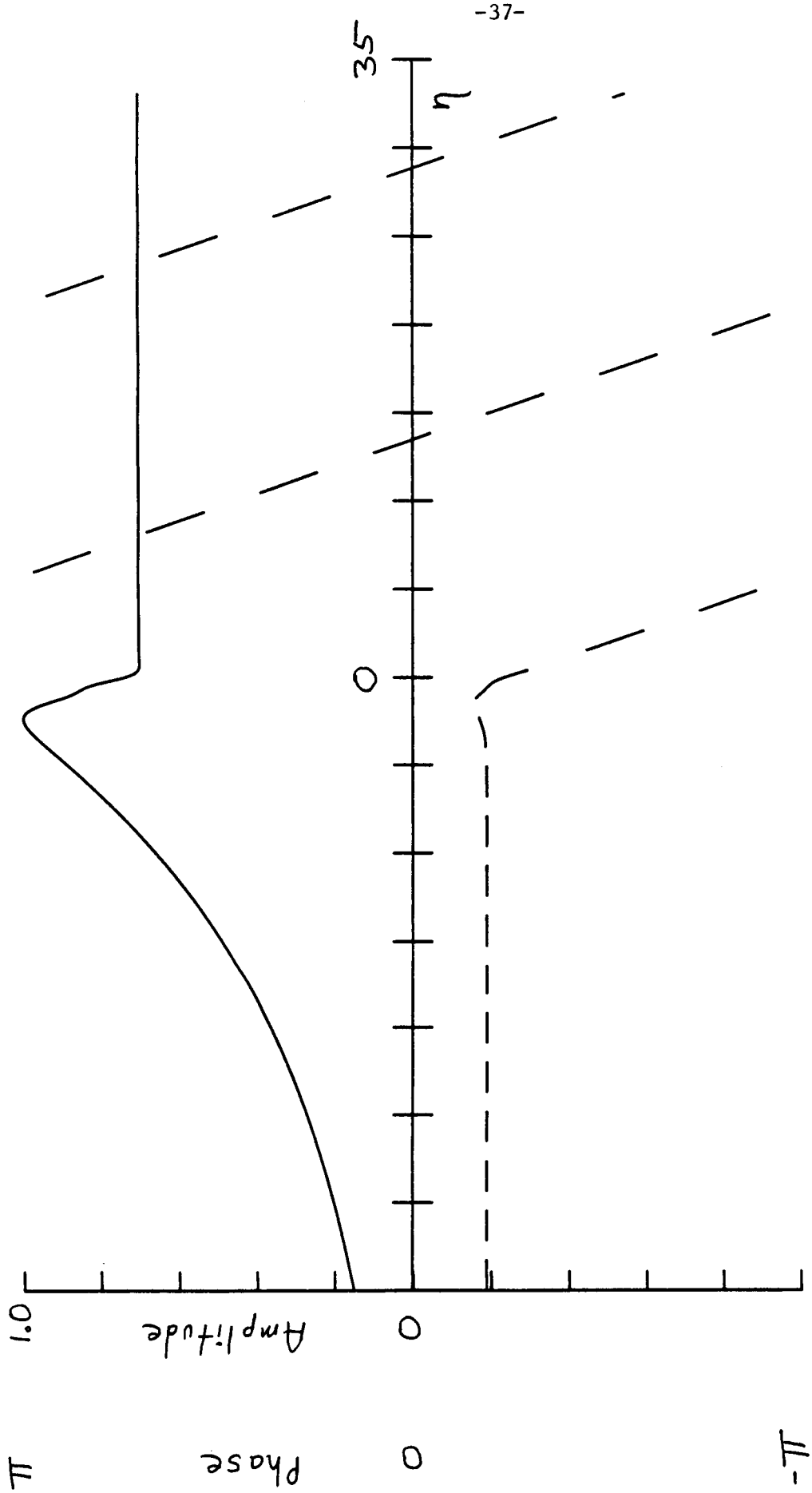

Figure 22. Plot of the two dimensional slow supersonic neutral eigenfunction $\Pi(\eta)$ along the contour $\eta = \eta_r - i$. The solid curve corresponds to the amplitude and the dashed curve to the phase. M = 5, β_T = 1: Lock Model; ω_N = 0.015708, α_N = 0.097492, c_N = 0.161113.

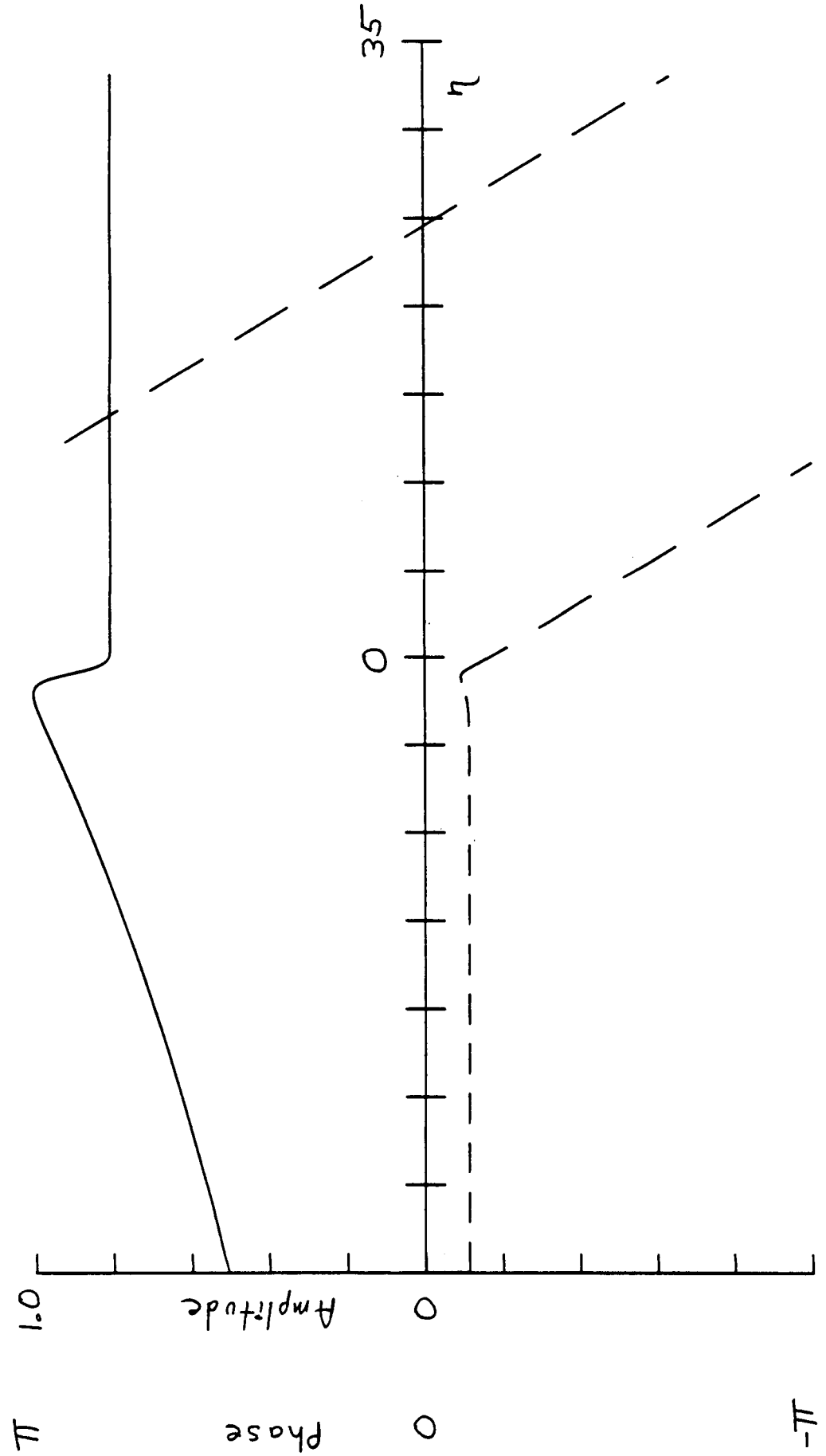

Figure 23. Plot of the two dimensional slow supersonic neutral eigenfunction $\Pi(\eta)$ along the contour $\eta = \eta_r - i$. The solid curve corresponds to the amplitude and the dashed curve to the phase. M = 5, $\beta_T = 1$: Sutherland Model; $\omega_N = 0.010800$, $\alpha_N = 0.057794$, $c_N = 0.186871$.

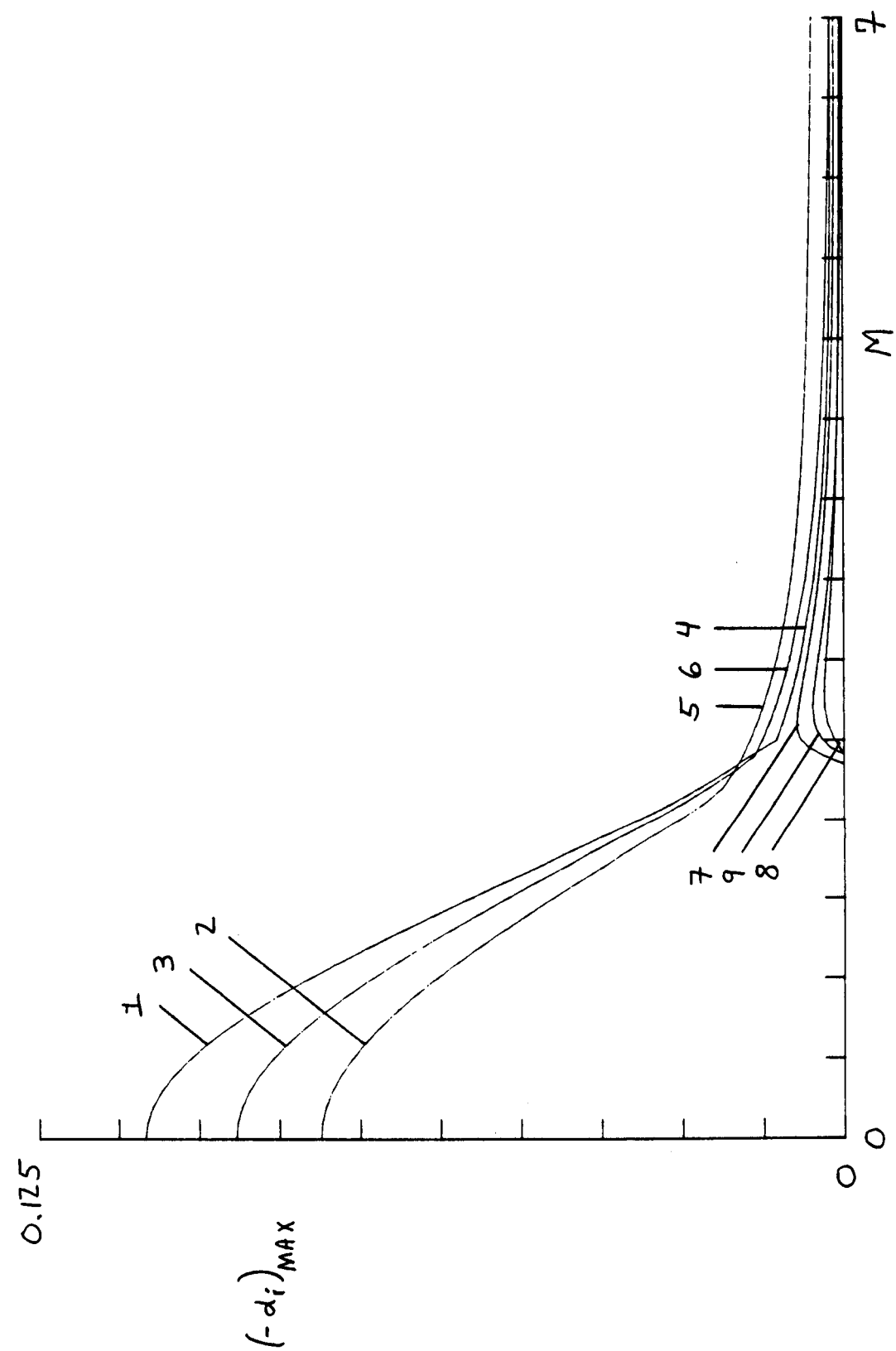

Figure 24. Plot of maximum growth rates of the two dimensional modes versus Mach number for $\beta_T = 2.0$. Subsonic Modes: (1) Tanh, (2) Lock, (3) Sutherland; Fast Modes: (4) Tanh, (5) Lock, (6) Sutherland; Slow modes: (7) Tanh, (8) Lock, (9) Sutherland.

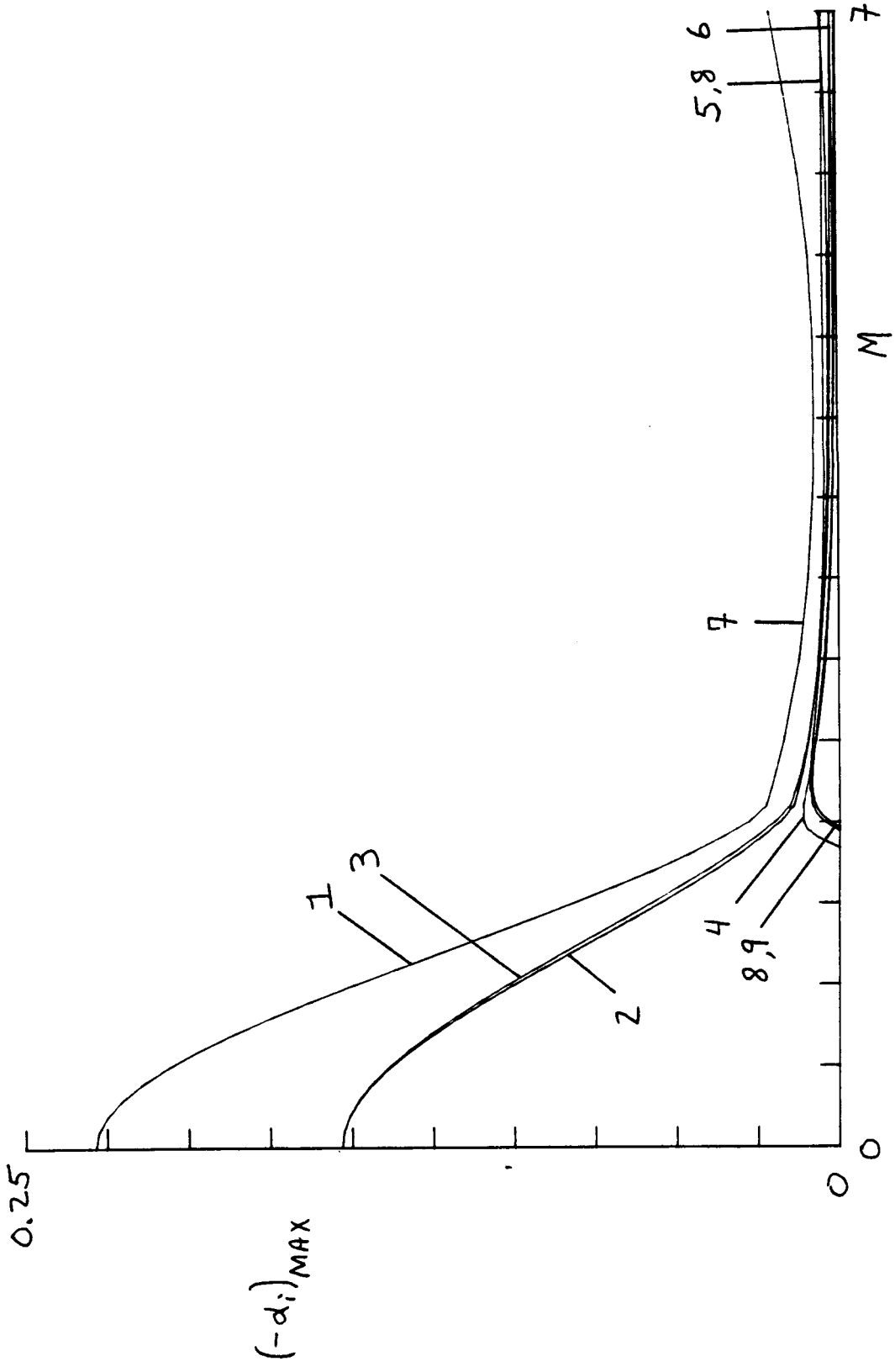

Figure 25. Plot of maximum growth rates of the two dimensional modes versus Mach number for β_T = 1.0. Subsonic Modes: (1) Tanh, (2) Lock, (3) Sutherland; Fast Modes: (4) Tanh, (5) Lock, (6) Sutherland; Slow modes: (7) Tanh, (8) Lock, (9) Sutherland.

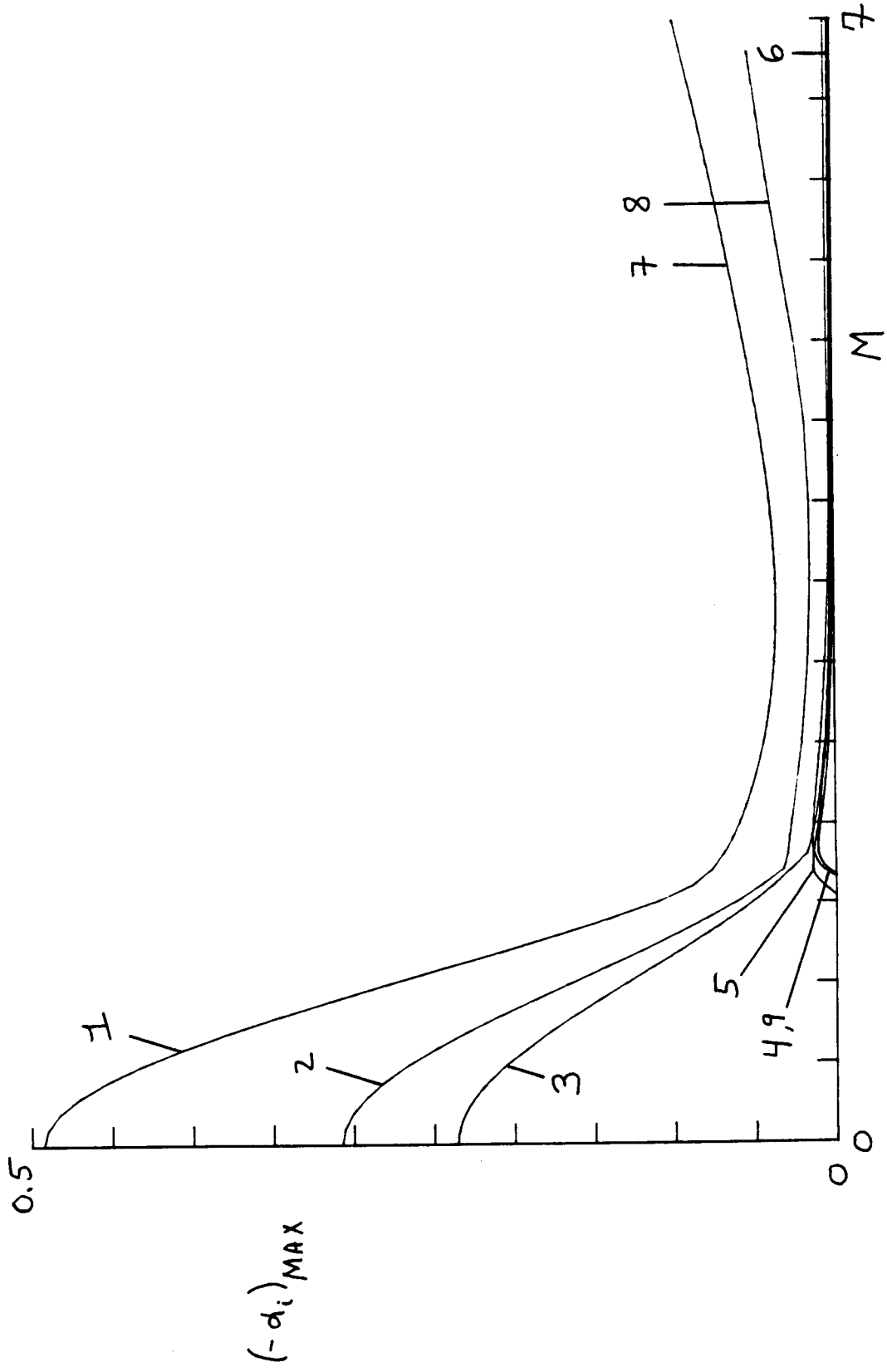

Figure 26. Plot of maximum growth rates of the two dimensional modes versus Mach number for $\beta_T = 0.5$. Subsonic Modes: (1) Tanh, (2) Lock, (3) Sutherland; Fast Modes: (4) Tanh, (5) Lock, (6) Sutherland; Slow modes: (7) Tanh, (8) Lock, (9) Sutherland.

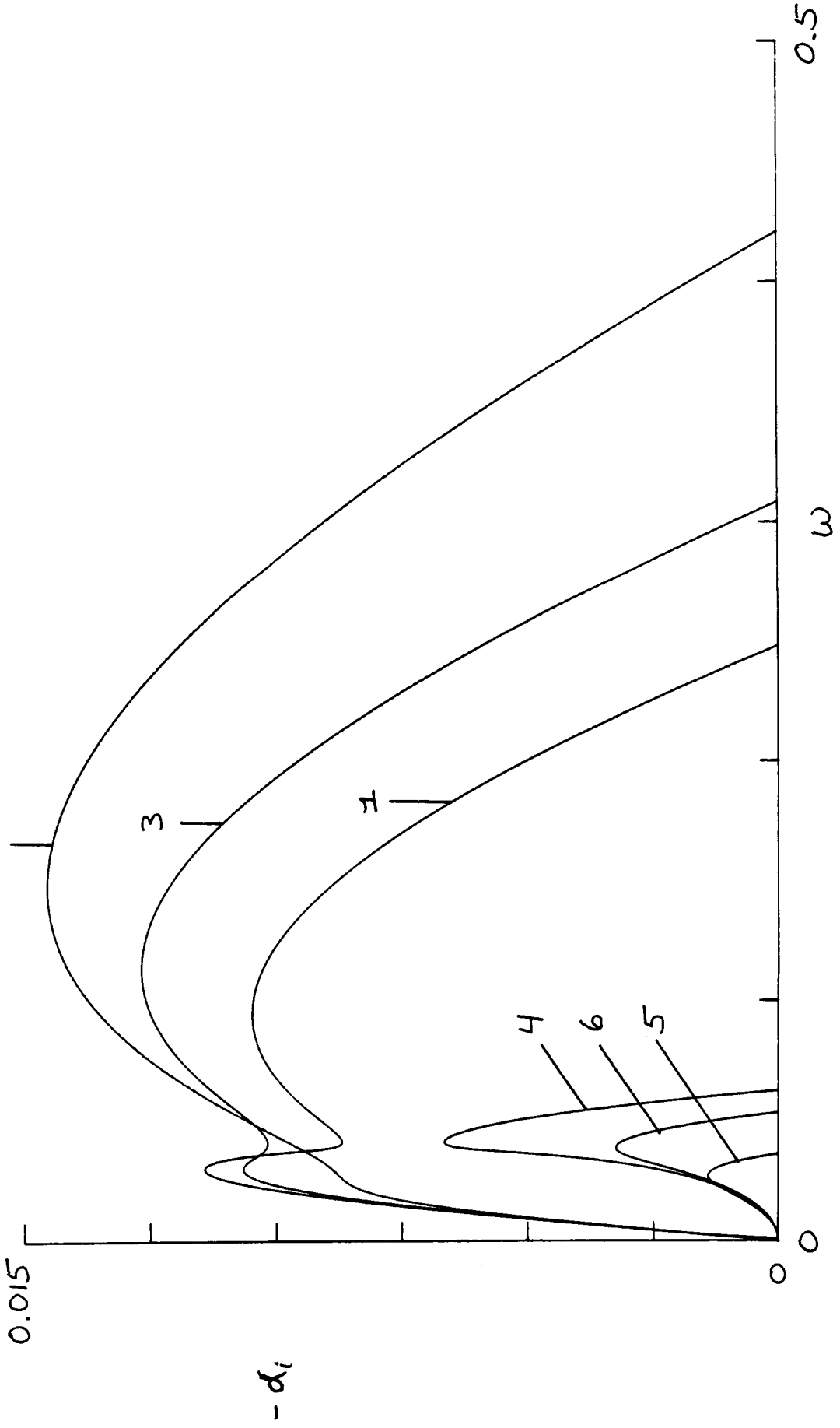

Figure 27. Plot of growth rates $-\alpha_i$ of the fast and slow two dimensional modes versus frequency for $\beta_T = 2$ and M = 2.5. Fast Modes: (1) Tanh, (2) Lock, (3) Sutherland; Slow Modes: (4) Tanh, (5) Lock, (6) Sutherland.

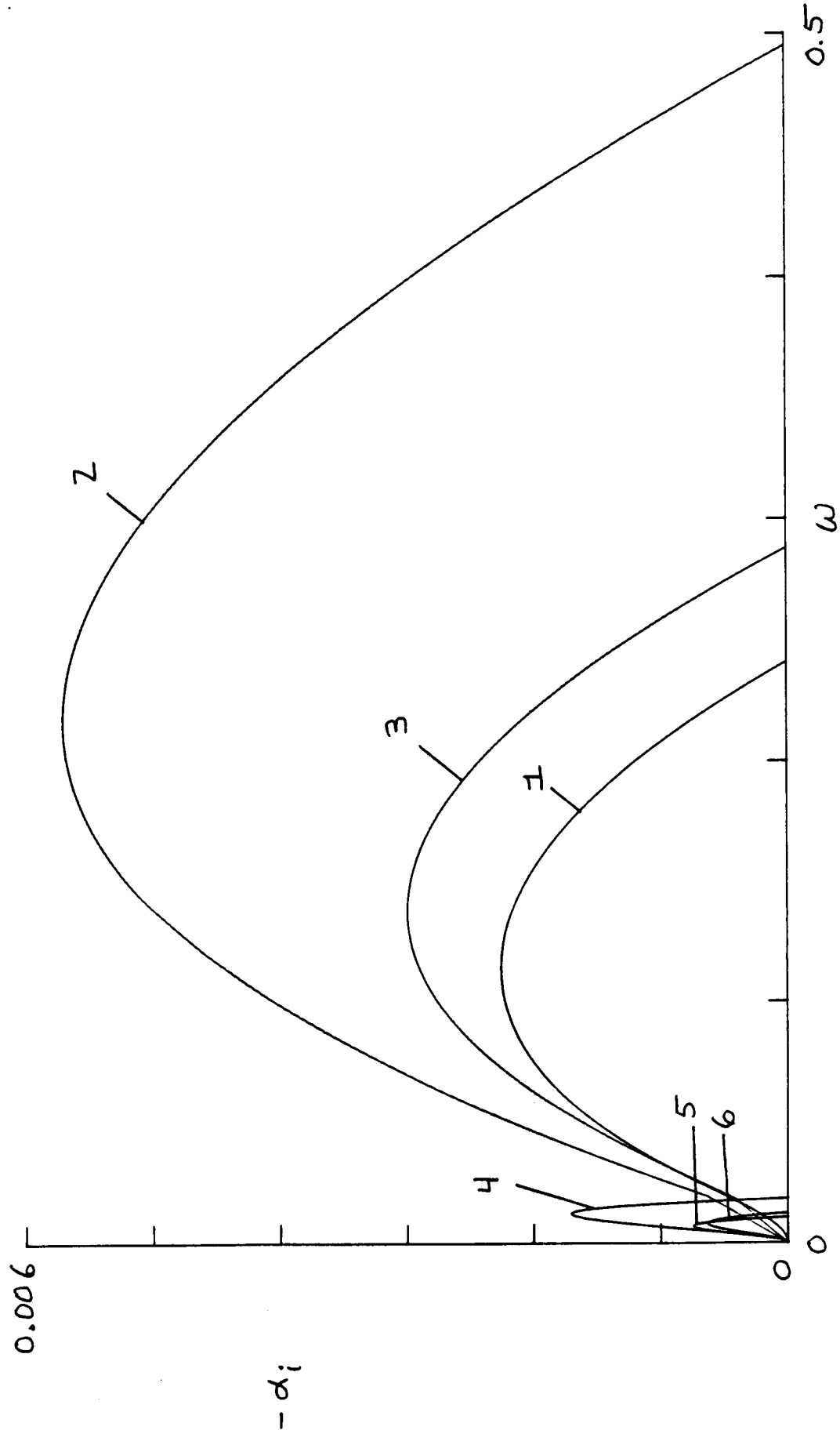

Figure 28. Plot of growth rates $-\alpha_i$ of the fast and slow two dimensional modes versus frequency for $\beta_T = 2$ and M = 5.0. Fast Modes: (1) Tanh, (2) Lock, (3) Sutherland; Slow Modes: (4) Tanh, (5) Lock, (6) Sutherland.

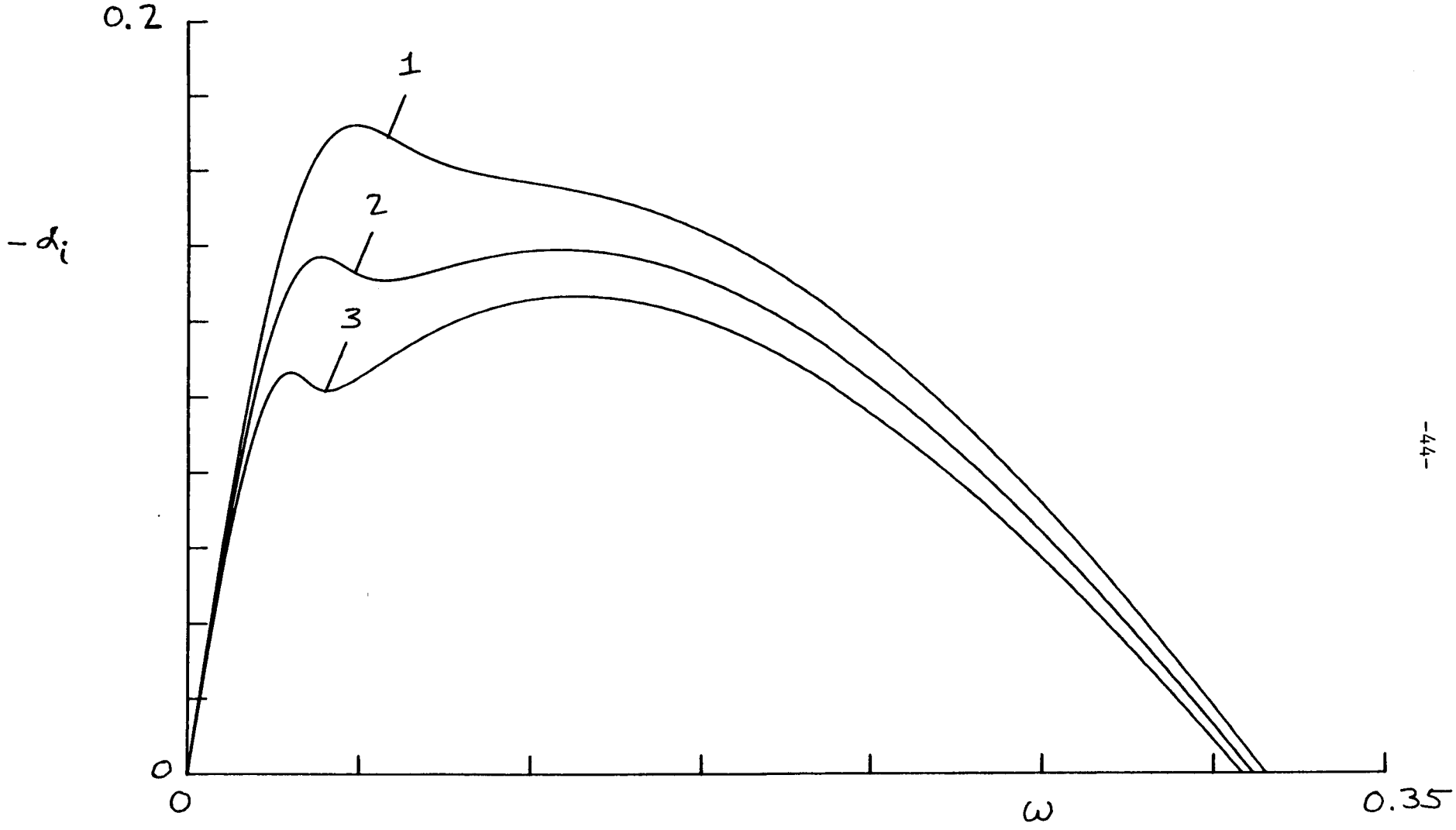

Figure 29. Plot of growth rates $-\alpha_i$ of the fast two dimensional modes versus frequency for $\beta_T = 2$ and Sutherland Model with Pr = 0.7. Mach numbers: (1) 2.3, (2) 2.4, (3) 2.5.

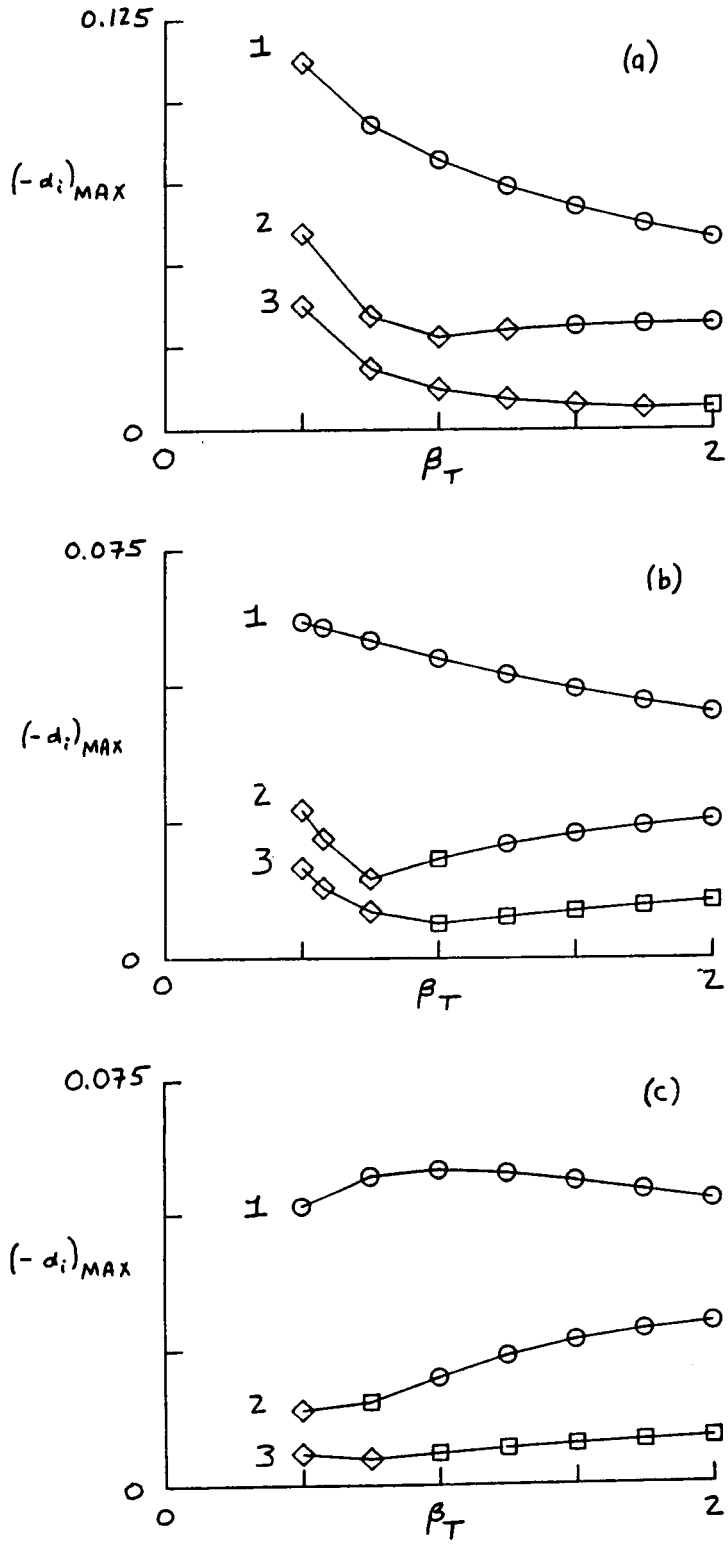

Figure 30. Plot of maximum growth rates versus β_T for Mach numbers (1) 1.5, (2) 2.0, (3) 3.0 for Subsonic (o), Fast Supersonic (□), and Slow Supersonic (◇) Modes; (a) Tanh, (b) Lock, (c) Sutherland.

NASA
National Aeronautics and Space Administration

Report Documentation Page

1. Report No.	2. Government Accession No.	3. Recipient's Catalog No.
NASA CR-181855 ICASE Report No. 89-32		

4. Title and Subtitle

INVISCID SPATIAL STABILITY OF A COMPRESSIBLE MIXING LAYER. PART III. EFFECT OF THERMODYNAMICS

5. Report Date

June 1989

6. Performing Organization Code

7. Author(s)

T. L. Jackson
C. E. Grosch

8. Performing Organization Report No.

89-32

10. Work Unit No.

505-90-21-01

9. Performing Organization Name and Address

Institute for Computer Applications in Science and Engineering
Mail Stop 132C, NASA Langley Research Center
Hampton, VA 23665-5225

11. Contract or Grant No.

NAS1-18605

13. Type of Report and Period Covered

Contractor Report

12. Sponsoring Agency Name and Address

National Aeronautics and Space Administration
Langley Research Center
Hampton, VA 23665-5225

14. Sponsoring Agency Code

15. Supplementary Notes

Langley Technical Monitor:
Richard W. Barnwell

Final Report

Journal of Fluid Mechanics

16. Abstract

We report the results of a comprehensive comparative study of the inviscid spatial stability of a parallel compressible mixing layer using various models for the mean flow. The models are (a) the hyperbolic tangent profile for the mean speed and the Crocco relation for the mean temperature, with the Chapman viscosity-temeprature relation and a Prandtl number of one; (b) the Lock profile for the mean speed and the Crocco relation for the mean temperature, with the Chapman viscosity-temperature relation and a Prandtl number of one; and (c) the similarity solution for the coupled velocity and temperature equations using the Sutherland viscosity temperature relation and arbitrary but constant Prandtl number. The purpose of this study was to determine the sensitivity of the stability characteristics of the compressible mixing layer to the assumed theromdynamic properties of the fluid. It is shown that the quantative differences resulting from the difference in the thermodynamic models. In particular, we show that the stability characteristics are sensitive to the value of the Prandtl number.

17. Key Words (Suggested by Author(s))	18. Distribution Statement
mixing layer, thermodyamics, spatial stability	34 - Fluid Mechanics Unclassified - unlimited

19. Security Classif. (of this report)	20. Security Classif. (of this page)	21. No. of pages	22. Price
Unclassified	Unclassified	46	A03

NASA FORM 1626 OCT 86